Report of Investigation 2025-4

TSUNAMI INUNDATION MAP OF FALSE PASS, ALASKA

Elena N. Troshina, J. Barrett Salisbury, and Dmitry J. Nicolsky

Published by
STATE OF ALASKA
DEPARTMENT OF NATURAL RESOURCES
DIVISION OF GEOLOGICAL & GEOPHYSICAL SURVEYS
2025

TSUNAMI INUNDATION MAP OF FALSE PASS, ALASKA

Elena N. Troshina, J. Barrett Salisbury, and Dmitry J. Nicolsky

Report of Investigation 2025-4

State of Alaska
Department of Natural Resources
Division of Geological & Geophysical Surveys

STATE OF ALASKA
Mike Dunleavy, Governor

DEPARTMENT OF NATURAL RESOURCES
John Boyle, Commissioner

DIVISION OF GEOLOGICAL & GEOPHYSICAL SURVEYS
Jennifer Athey, Acting State Geologist and Director

Publications produced by the Division of Geological & Geophysical Surveys (DGGS) are available for free download from the DGGS website (dggs.alaska.gov). Publications on hard-copy or digital media can be examined or purchased in the Fairbanks office:

Alaska Division of Geological & Geophysical Surveys
3354 College Rd., Fairbanks, Alaska 99709-3707
Phone: (907) 451-5010 Fax (907) 451-5050
dggspubs@alaska.gov | dggs.alaska.gov

DGGS publications are also available at:
Alaska State Library,
Historical Collections & Talking Book Center
395 Whittier Street
Juneau, Alaska 99811

Alaska Resource Library and Information Services (ARLIS)
3150 C Street, Suite 100
Anchorage, Alaska 99503

Suggested citation:
Troshina, E.N., Salisbury, J.B., and Nicolsky, D.J., 2025, Tsunami inundation map of False Pass, Alaska: Alaska Division of Geological & Geophysical Surveys Report of Investigation 2025-4, 38 p., 1 sheet, 1:10.000 scale. https://doi.org/10.14509/31682

Cover photo. False Pass, Alaska.

Contents

Figures

Tables

Appendix

Map Sheets

TSUNAMI INUNDATION MAP OF FALSE PASS, ALASKA

Elena N. Troshina[1], J. Barrett Salisbury[2], and Dmitry J. Nicolsky[1]

Abstract

We evaluate potential tsunami hazards for the community of False Pass, Alaska, by numerically modeling the extent of inundation from tsunami waves generated by hypothetical earthquakes. We define an updated suite of earthquakes—including Tohoku-style megathrust ruptures and other sources in the western Alaska Peninsula region—to calculate vertical seafloor displacements and model resulting tsunami dynamics. A hypothetical earthquake with maximum slip distributed between depths of 10 and 20 km (6.2 and 12.4 mi) results in "worst case" tsunami inundation in False Pass. If the tsunami arrives at high tide, the maximum predicted overland flow depths in the community can reach up to 10 m (32.8 ft), and the currents could be as strong as 15 m/sec (29 knots). Dangerous wave activity is expected to last for more than 12 hours. Results presented here are intended to provide guidance to local emergency management agencies for tsunami inundation assessment, evacuation planning, and public education to mitigate future tsunami damage.

INTRODUCTION

Subduction of the Pacific plate under the North American plate has resulted in numerous great (M > 8) earthquakes and is the source of locally generated tsunamis in Alaska (Dunbar and Weaver, 2008). During the 20th century, several tsunamis generated by Alaska–Aleutian subduction zone earthquakes have resulted in widespread damage and loss of life in exposed coastal communities across the Pacific Ocean basin (Lander, 1996). In this report, we focus on tsunamis originating in the vicinity of the western Alaska Peninsula (WAP) and eastern Aleutian Islands (fig. 1) as near-field hazards with the potential to reach Alaska's coastal communities within minutes of an earthquake. Reducing property damage and loss of life is highly dependent on community preparedness.

Despite the relatively recent sequence of large and great earthquakes (1938, 1946, 1957, 1964; fig.1), the region still has high potential for future large earthquakes, and it is only a matter of time before another devastating tsunami occurs (Kirby and others, 2013). Thus, estimating the potential flooding of the coastal zone in the next local or distant tsunami event is an essential component of the preparedness process. Combined with high-resolution continuous global positioning system (GNSS and GPS) measurements and recent paleoseismic studies along the southern Alaska coast, the lessons learned from tsunami disasters of 2004 in Indonesia and 2011 in Japan have helped improve our understanding of complex earthquake source mechanisms. Consequently, we include new potential earthquake sources in our tsunami analysis to

[1] Alaska Earthquake Center, Geophysical Institute, University of Alaska, P.O. Box 757320, Fairbanks, Alaska 99775
[2] Alaska Division of Geological & Geophysical Surveys, 3354 College Road, Fairbanks, Alaska 99709

develop the worst-case credible tsunami scenarios for False Pass. This report does not include subaerial or submarine landslide-generated tsunami events.

The tsunami inundation map of False Pass described in this report represents the results of a continuous, combined effort of state and federal agencies to mitigate tsunami damage in coastal Alaska. The intended audience of this report is scientists, engineers, emergency managers, and community planners interested in an applied approach to developing tsunami inundation and evacuation maps. Digital data and documentation provided with the report enable technical users to explore the range of possible tsunami inundation for potential events. We use a deterministic approach for our earthquake and tsunami hazard modeling, which is distinctly different from the probabilistic tsunami hazard analysis used in projects with different objectives, such as land-use planning or insurance estimates (Geist and Parsons, 2006). We are less concerned about the probability that an earthquake of a certain magnitude will occur in a given amount of time and are more focused on the community-specific tsunami inundation that might result from the largest hypothetical, yet scientifically plausible earthquake scenarios. The methods used to develop tsunami inundation maps are described in detail in multiple publications and are not reviewed in this report. Refer to Suleimani and others (2016) for a complete description of the process.

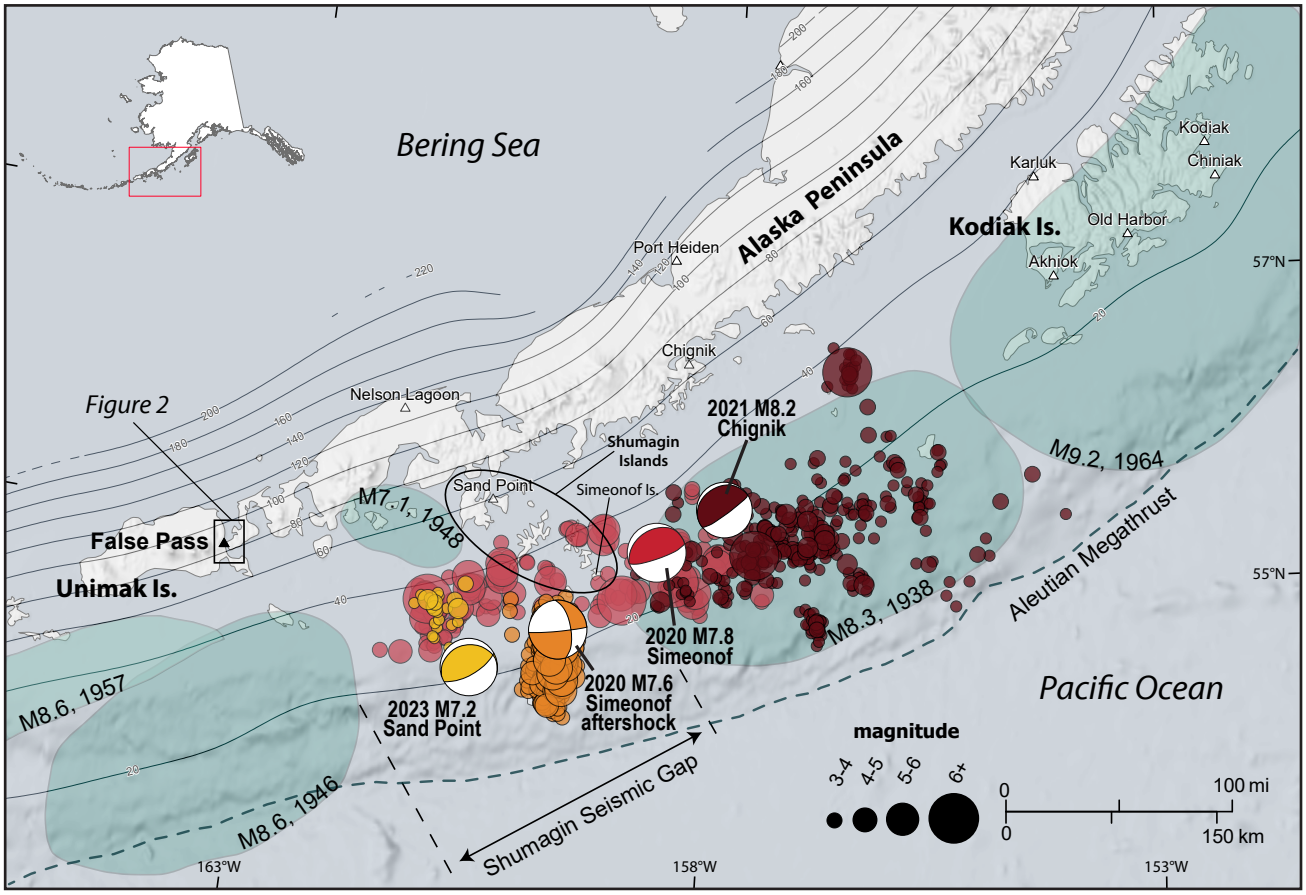

Figure 1. Map of western Alaska Peninsula and Unimak Island showing the location of False Pass; the rupture zones of the 1938, 1946, 1948, 1957, and 1964 megathrust earthquakes (gray-green shaded areas); and four recent major earthquakes from the Shumagin seismic gap with their focal mechanisms and aftershocks, color-coded by sequence. The bold dashed line defines the Aleutian Megathrust and thin, solid lines represent depth contours of the plate interface with a 20-km interval.

PROJECT BACKGROUND: REGIONAL AND HISTORICAL CONTEXT

Setting

The following information is from the Alaska Community Database maintained by the State of Alaska, Department of Commerce, Community, and Economic Development, Division of Community and Regional Affairs (DCCED/DCRA, 2015).

False Pass (54°49'40"N, 163°23'57"W), population 60, is on the eastern end of Unimak Island on the Isanotski Strait that connects the Pacific Ocean to the Bering Sea; another part of the community is across the strait on the westernmost tip of the Alaska Peninsula (figs. 1 and 2). False Pass is 1,040 km (646 mi) southwest of Anchorage and 322 km (200 mi) east of Dutch Harbor. The area was originally settled by a homesteader in the early 1900s, and the first cannery was established in 1917. Alaska Natives immigrated to False Pass from other places when the cannery was built. The cannery operated almost continuously until it was destroyed by fire in 1981. The city was incorporated in 1990. False Pass is a federally recognized tribe with primarily Unangan members. Fishing, fish processing, and subsistence activities are major parts of the lifestyle. Boat and aircraft are the only ways to get to False Pass.

Seismic History

Unimak Island is the easternmost island in the Aleutian chain (fig. 1). This island arc constitutes the boundary along which the Pacific and North American plates converge and form the Alaska–Aleutian subduction zone (AASZ), also known as the Aleutian Megathrust. The Shumagin Islands archipelago of about 20 islands is in the same area (black oval, fig. 1). The rate of plate convergence near the archipelago is approximately 63–66 mm (2.5–2.6 in) per year (DeMets and others, 1990; Page and others, 1991; Argus and others, 2010), and the Alaska Peninsula segment of the megathrust has produced some significant tsunamigenic earthquakes in the period of 1938–1964 (gray-green shaded polygons, fig. 1). However, during this period, a region of the megathrust between the 1938 and 1946 plate boundary earthquakes did not rupture and has been called the Shumagin seismic gap. In addition to having no great ($M > 8$) earthquakes from 1938–1964, this seismic gap separates the fully creeping section of the plate interface to the west from the fully coupled Kodiak segment to the east (Elliott and others, 2022). Refer to "Seismic and Tsunami History" in Nicolsky and others (2017) and Elliott and others (2022) for a detailed description of these events and a summary of the tectonic regime around the Shumagin seismic gap area in the last century.

More recently, between 2020 and 2024, four closely spaced earthquakes greater than magnitude 7.0 ruptured within or near the Shumagin seismic gap offshore of the Alaska Peninsula (fig. 1). The first of these, the July 22, 2020, M7.8 Simeonof earthquake and its aftershocks (red plots, fig. 1), overlapped the western portion of the 1938 rupture patch and about 75 percent of the Shumagin seismic gap, which had not ruptured since 1917 (Liu and others, 2020). The earthquake and its aftershock sequence did not completely fill the seismic gap, leaving the western third of the gap adjacent to the 1946 earthquake unbroken. The focal mechanism determined by the Global Centroid Moment tensor (GCMT) indicates that the earthquake occurred on a shallow thrust, consistent with a rupture of the well-determined slab interface.

Three months later, on October 19, 2020 , the M_W 7.6 Simeonof aftershock ruptured on a nearly north–south-oriented fault plane with a strike-slip faulting mechanism to the west of the main event, triggered by the mainshock and subsequent afterslip (Zhao and others, 2022).

The following year on July 29, 2021, the M_W 8.2 Chignik megathrust earthquake ruptured the subduction zone immediately east of the 2020 Simeonof rupture zone at a similar range of depth as the 2020 Simeonof event (maroon plots, fig.

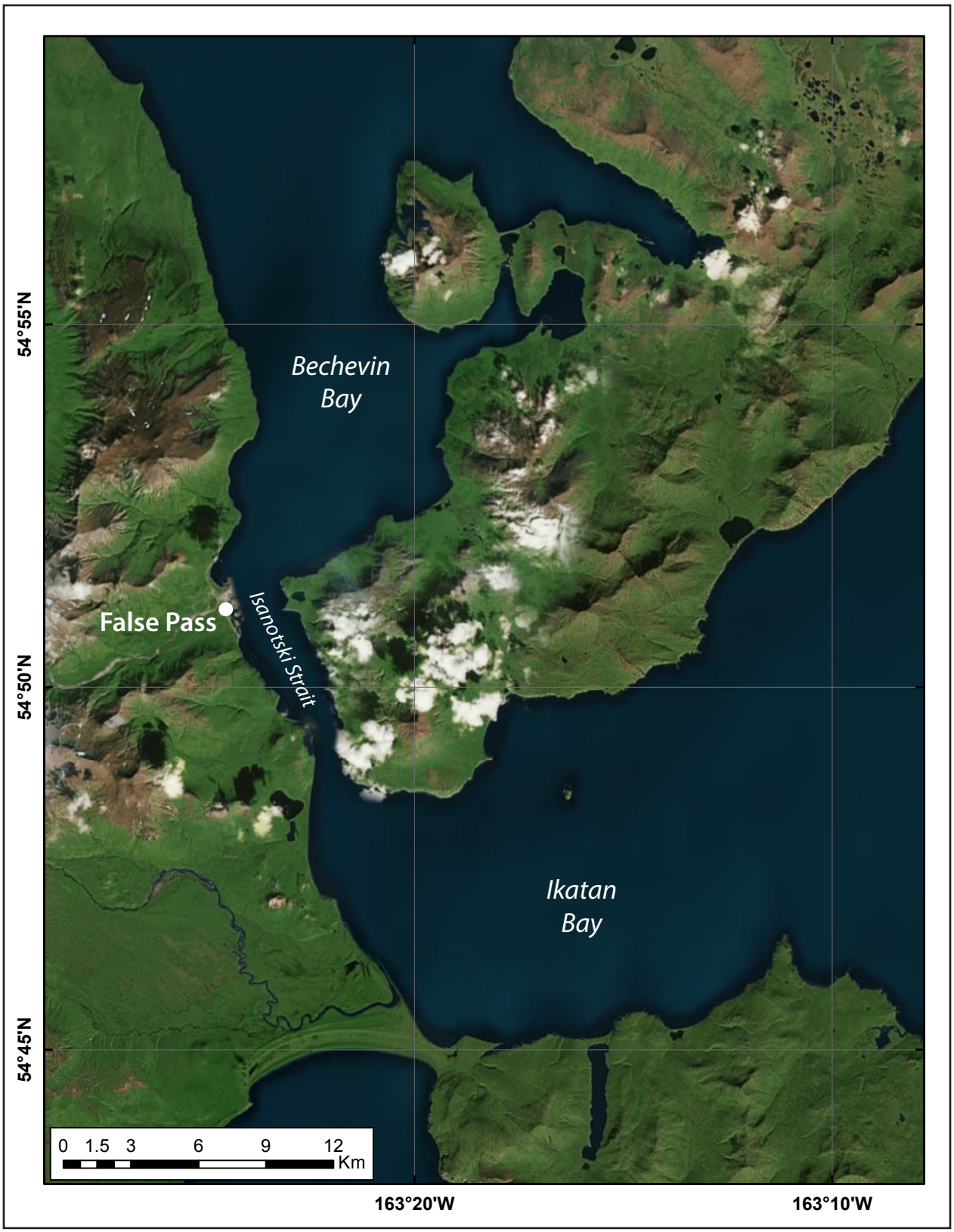

Figure 2. Satellite imagery of Isanotski Strait that separates Unimak Island from the Alaska Peninsula, with False Pass shown on Unimak Island.

1). The Chignik earthquake was the largest event in the United States since the 1965 M8.7 Rat Islands earthquake. Both earthquakes, a year apart, mostly ruptured the 20- to 40-km depth range within segments of the interface that appear to be partially coupled and thus did not trigger substantial tsunamis (Elliott and others, 2022).

Continuing this sequence of large earthquakes, on July 15, 2023, the magnitude 7.2 Sand Point earthquake (yellow plots, fig. 1) ruptured within the M7.8 Simeonof aftershock zone. Its source mechanism is similar to the Simeonof event and indicates fault rupture along the Aleutian megathrust. The 2020–2023 earthquake sequence of four large earthquakes partially filled the Shumagin seismic gap.

Tsunami History

Both Lander (1996) and the National Centers for Environmental Information (NCEI) Global Historical Tsunami Database (National Geophysical Data Center, continuously updated) list only one event in which False Pass was affected by tsunami waves. On April 1, 1946, a strong M_W 8.6 earthquake (Lopez and Okal, 2006) near Unimak Island triggered a major destructive tsunami in the Pacific Ocean. Local waves reached 42 m (138 ft) in height on Unimak Island and 1.5 m (5 ft) in False Pass. Light damage and scattered pilings were reported at the False Pass cannery. Several other earthquakes and tsunamis have likely affected the area around False Pass; however, no records of events prior to 1946 are currently available.

Historical records, unfortunately, are usually too short to sample the variability of slip on the megathrust (Stein and Okal, 2007). Paleotsunami and paleoseismic studies have the potential to extend records back in time and thus help to develop hypothetical maximum credible scenarios. To document tectonic deformation in the outer Shumagin Islands, Witter and others (2014) performed a paleoseismic study on Simeonof Island (fig. 1), the island closest to the trench. This investigation determined that there was no evidence for either sudden coseismic land-level changes produced by great earthquakes or any trace of marine deposits left by high tsunamis (Witter and others, 2014). The authors concluded that the lack of geologic evidence for great earthquakes and tsunamis on Simeonof Island indicates that aseismic slip may accommodate a substantial component of plate convergence along the Shumagin segment over the past 3,400 years. Witter and others (2014) suggested that large M7–M7.5 earthquakes might be sufficient to release the strain stored in the Shumagin seismic gap. The implications of this geologic/paleoseismologic study on the development of the hypothetical tsunami scenarios are discussed later in the report.

METHODOLOGY AND DATA

Grid Development and Data Sources

We use a series of nested computational grids on the coast of WAP and eastern Aleutian Islands to generate detailed maps of potential tsunami inundation triggered by local and distant earthquakes. The coarsest grid, Level 0, with 2-arc-minute (~2 km [~1.2 mi]) resolution, spans the central and northern Pacific Ocean (extent of the Level 0 grid is not shown in fig. 3). We used three intermediate grids between the coarsest- and highest-resolution grids (table 1; fig. 3). The highest-resolution grid (level 4, shaded rectangle, fig. 3) covers coastal waters next to the community. The spatial resolution of the level 4 grid, with cell dimensions of about 13.2 × 16.4 m (43.3 × 53.8 ft), satisfies National Oceanic and Atmospheric Administration (NOAA) minimum recommended requirements for computation of tsunami inundation (National Tsunami Hazard Mapping Program [NTHMP], 2010).

The map sheet included in this report shows the maximum composite extent of inundation for all considered tsunami scenarios and the maximum composite flow depths over dry land. The composite values are calculated as follows: for each tsunami scenario, the tsunami flow depth is computed at each grid point, and at every time step during the tsunami propagation time the maximum value is

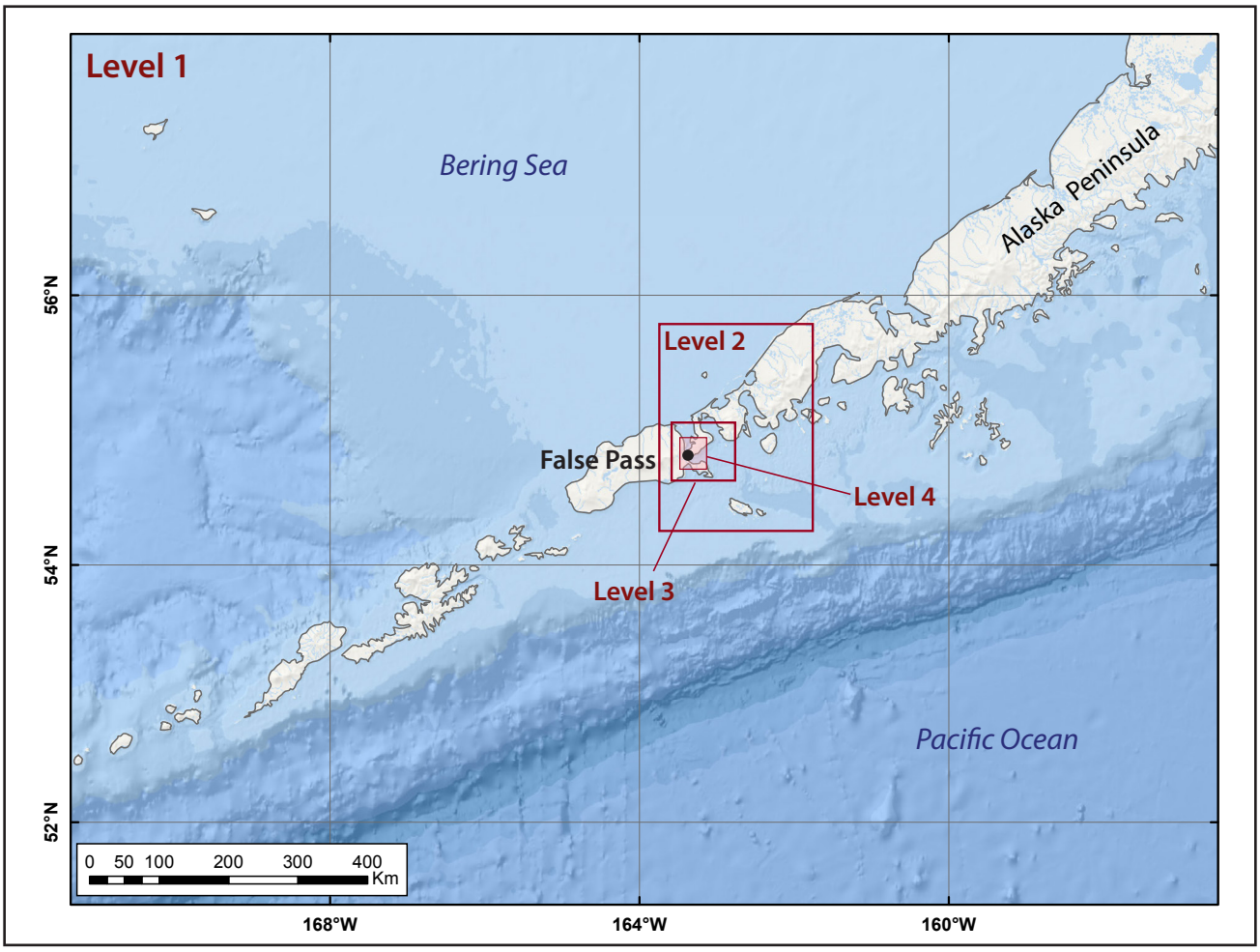

Figure 3. Nesting of the levels 1–4 bathymetry/topography grids for numerical modeling of tsunami propagation and runup in False Pass. Each embedded grid is outlined by a red rectangle. The shaded rectangle is the high-resolution level 4 grid.

Table 1. Nested grids used to compute propagation of tsunami waves to False Pass. The high-resolution grid is used to compute the inundation. Note that the grid resolution in meters is not uniform; the first dimension is the longitudinal grid resolution and the second is the latitudinal resolution.

Grid name	Resolution		West–East boundaries	South–North boundaries
	arc-seconds	meters (feet)		
Level 0, Northern Pacific	120 × 120	≈ 2,935 × 3,700 (9,629 × 12,139)	120°00' E–60°00' W	60°00' S–65°00' N
Level 1, Eastern Aleutians	24 × 24	≈ 427 × 740 (1,401 x 2,428)	171°58' W–157°02' W	51°20' N–57°28' N
Level 2, Coarse resolution, False Pass	8 × 8	≈ 142 x 247 (466 x 810)	161°47'44" W–163°48'42" W	54°14'35" N–55°30'14" N
Level 3, Fine resolution, False Pass	8/3 × 8/3	≈ 48 × 82 (157 x 269)	162°50'51" W–163°28'45" W	54°37' N–54°58'56" N
Level 4, High resolution, False Pass	8/9 × 1/2	≈ 16 x 16 (52 × 52)	163°27'39" W–163°15'40" W	54°47'22" N–54°53'37" N

kept; then we compute the composite maximum flow depth from all considered scenarios by choosing the maximum value for each grid point among all scenarios. The same methodology is used to calculate the composite extent of tsunami inundation. The calculated extent of inundation accounts for coseismic deformation in the community. Refer to table 2 for maximum ground subsidence values associated with each earthquake scenario.

Numerical Model of Tsunami Propagation and Runup

To estimate tsunami runup in False Pass we used the same numerical modeling techniques as previous Alaska tsunami inundation studies (Suleimani and others, 2010, 2013, 2015, 2016, 2017; Nicolsky and others, 2011a, 2013, 2014, 2015, 2016). All hypothetical tsunami simulations were conducted using the bathymetric/topographic data corresponding to the Mean Higher High Water (MHHW) tide level. We use a conservative approach and assume that all simulated tsunamis arrive during high tides and with consideration to tectonic land-level changes (i.e., subsidence or uplift) caused by hypothetical earthquakes.

The numerical modeling results presented in this report are relevant for existing sea level conditions and do not account for changes in water levels caused by global sea level rise, regional tectonic processes, and isostatic rebound. Even though the report on global sea level changes for 2050 and 2100 by the Intergovernmental Panel on Climate Change (Oppenheimer and others, 2019) predicts global sea level rise, rapid regional uplift in southern Alaska caused by ice loss contributes to negative sea level changes in the region (Larsen and others, 2004; Shirzaei and others, 2021).

TSUNAMI SOURCES

Great historical earthquakes along the Alaska–Aleutian subduction zone occurred on the megathrust—the fault, or contact surface, between the subducting Pacific plate and the overriding North American plate (fig. 1). Friction between the two converging plates keeps them stuck, or "locked" together at the edges. Relative plate motion causes energy to accumulate at the plate boundaries and this energy is eventually released during sudden slip in an earthquake. It is theorized that the strain energy primarily accumulates in the locked, or coupled, patches of the megathrust where friction on the fault is greatest. Our goal is to evaluate the tsunami effects resulting from all plausible combinations of slip patches that may rupture in the next great earthquake.

The detailed description of the earthquake history and tectonic regime in the WAP region of the Alaska–Aleutian subduction zone (fig. 1) is given in Suleimani and others (2016).

To perform a comprehensive tsunami hazard assessment for False Pass, we consider variable slip distributions on neighboring segments of the interface—both along strike as well as at different depths. First, we conduct a sensitivity study to determine what effect the down-dip location of a rupture has on tectonic subsidence, uplift, and resulting tsunami waves. We then apply the results of the sensitivity study to construct the maximum credible scenarios.

Sensitivity Study

Earthquake ruptures with slip at different depths have different wave-generating potential, result in different distributions and amounts of subsidence and uplift in coastal communities, and therefore result in different tsunami and permanent flooding characteristics. The point of the sensitivity study is to determine the most dangerous location on the megathrust for a hypothetical earthquake to occur. We use the U.S. Geological Survey SLAB2 model of the Alaska–Aleutian plate interface developed by Hayes (2018). The plate interface is discretized into a mesh of rectangles ranging from 1 to 6 km (0.6 to 3.7 mi) in the along-strike direction of the plate interface, with denser discretization in its shallow part (fig. 4). The upper and lower edges of each rectangle coincide with depth contours of the plate interface that are spaced at

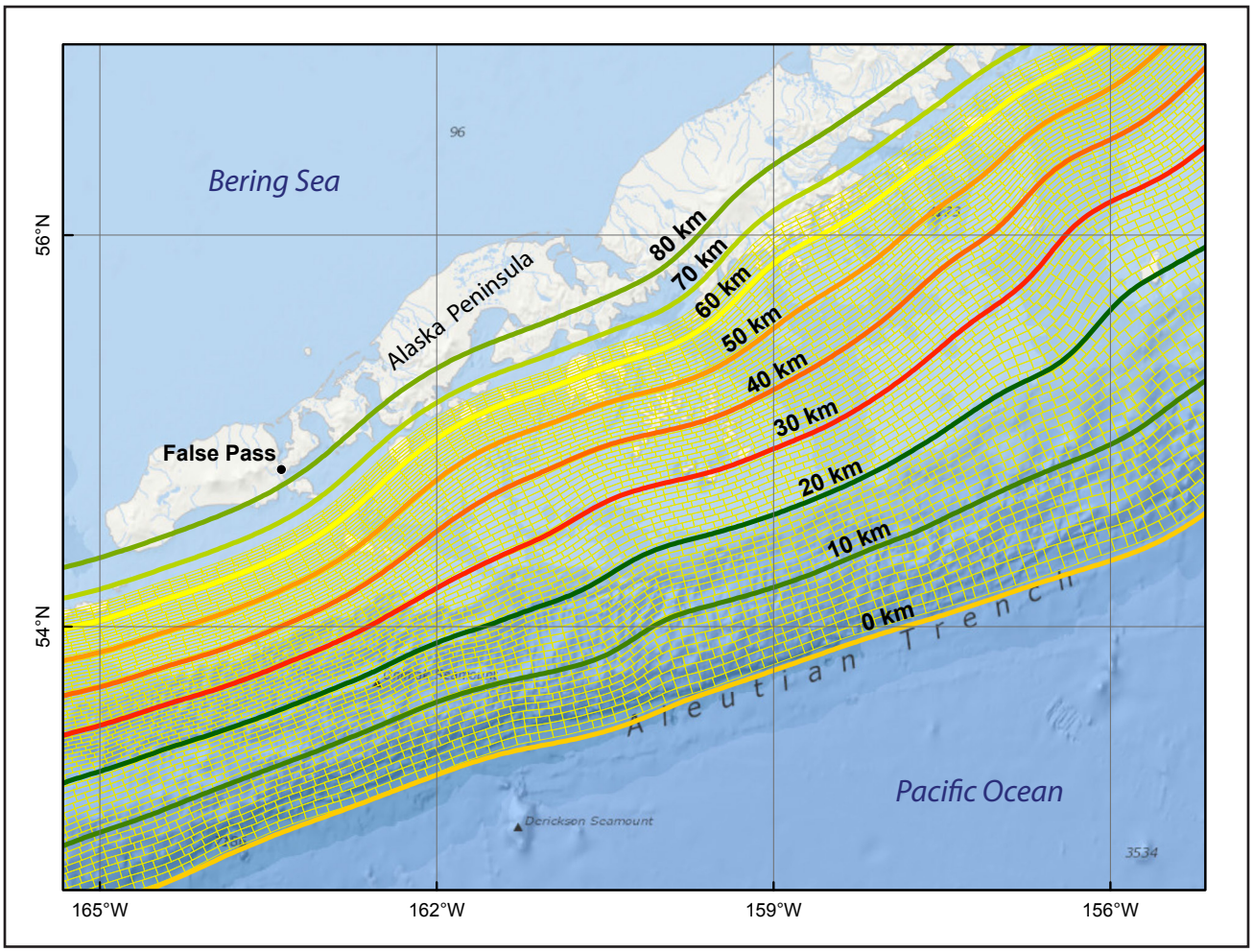

Figure 4. Discretization of the plate interface used to compute the coseismic vertical displacements with formulae developed by Okada (1985). Bold colored lines mark depth contours (in kilometers) of the plate interface, and the yellow rectangles represent individual subfaults that are used to construct an earthquake slip model.

0.5 km (0.3 mi), with spacing of 0.25 km (0.16 mi) at the shallowest part of the plate interface. The rectangles, called subfaults, are later used to compute coseismic ground deformation (Okada, 1985). Using this discretization of the plate interface, we model potential earthquake scenarios by prescribing a general pattern of slip distribution in the proposed rupture, then computing the slip at the center of each subfault using seismic moment (energy release) as a constraint.

We develop six different slip cases (A–F) for M_W 8.0 earthquakes and calculate vertical seafloor deformations associated with each case (fig. 5). The slip distribution for all six cases is uniform in the along-strike direction with tapering at the ends of the rupture. The assumed slip distribution is consistent with earthquake source scenarios used by other tsunami modeling studies (for example, Butler, 2014; USGS SAFRR scenario, www.usgs.gov/centers/western-geographic-science-center/science/safrr-tsunami-scenario). Between any two consecutive cases, the hypothetical rupture is offset by about 10 km (6.2 mi) in the downdip direction: case A corresponds to a shallow surface-breaching rupture with maximum slip located close to the trench; cases B, C, D, E, and F correspond to ruptures with maximum slip roughly centered at a depth of 10 km (6.2 mi), 20 km (12.4 mi), 30 km (18.6 mi), 40 km (24.8 mi), and 50 km (31 mi), respectively.

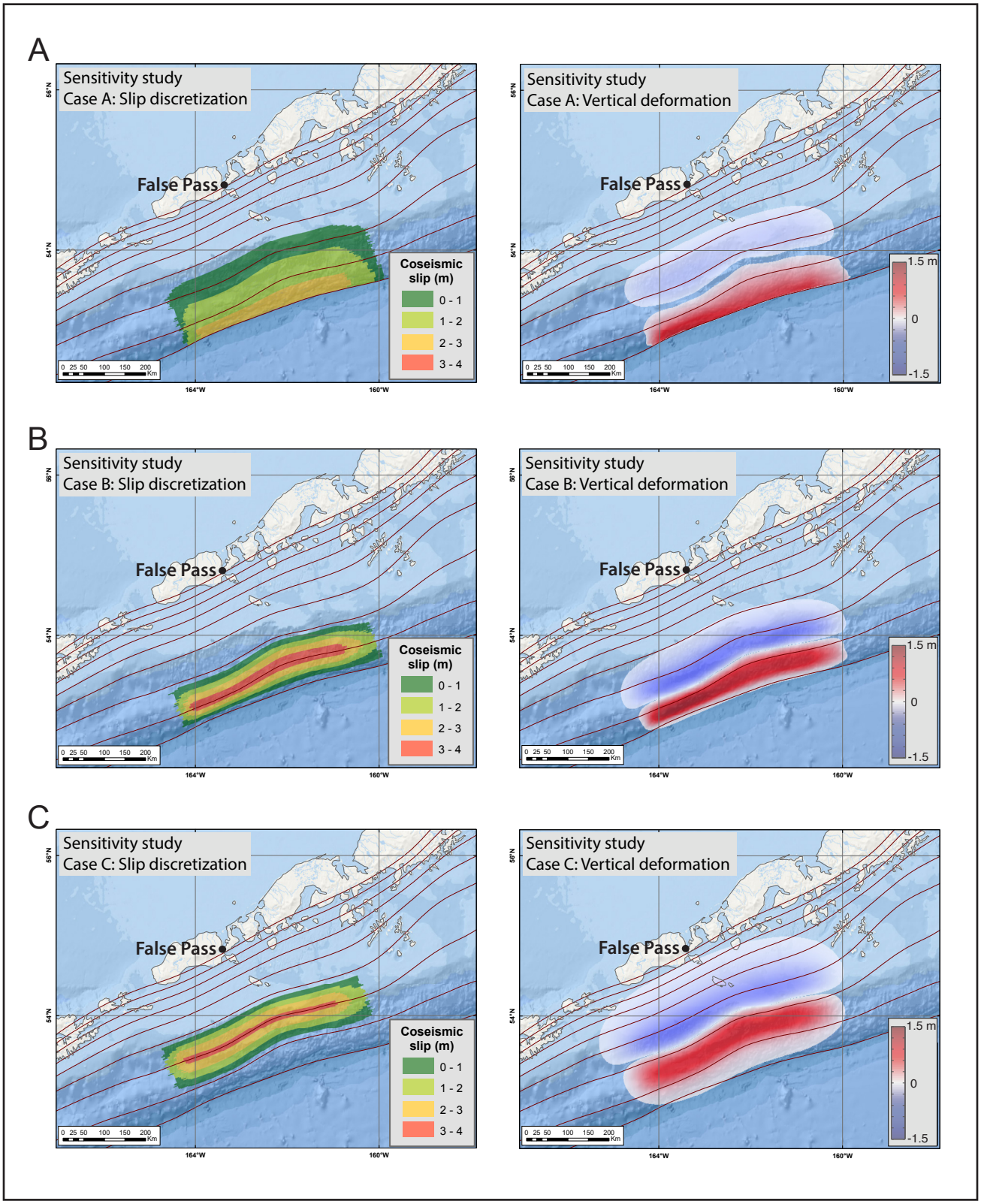

Figure 5. Imposed slip distributions along the plate interface (left) and computed vertical ground surface deformations (right) for sensitivity cases A–C, modeling M_W 8.0 ruptures near False Pass. The slip location varies in the downdip direction of the plate interface while preserving the same slip patch configuration. Brown lines are depth contours of the subduction interface from 0 to 80 km with a 10-km interval.

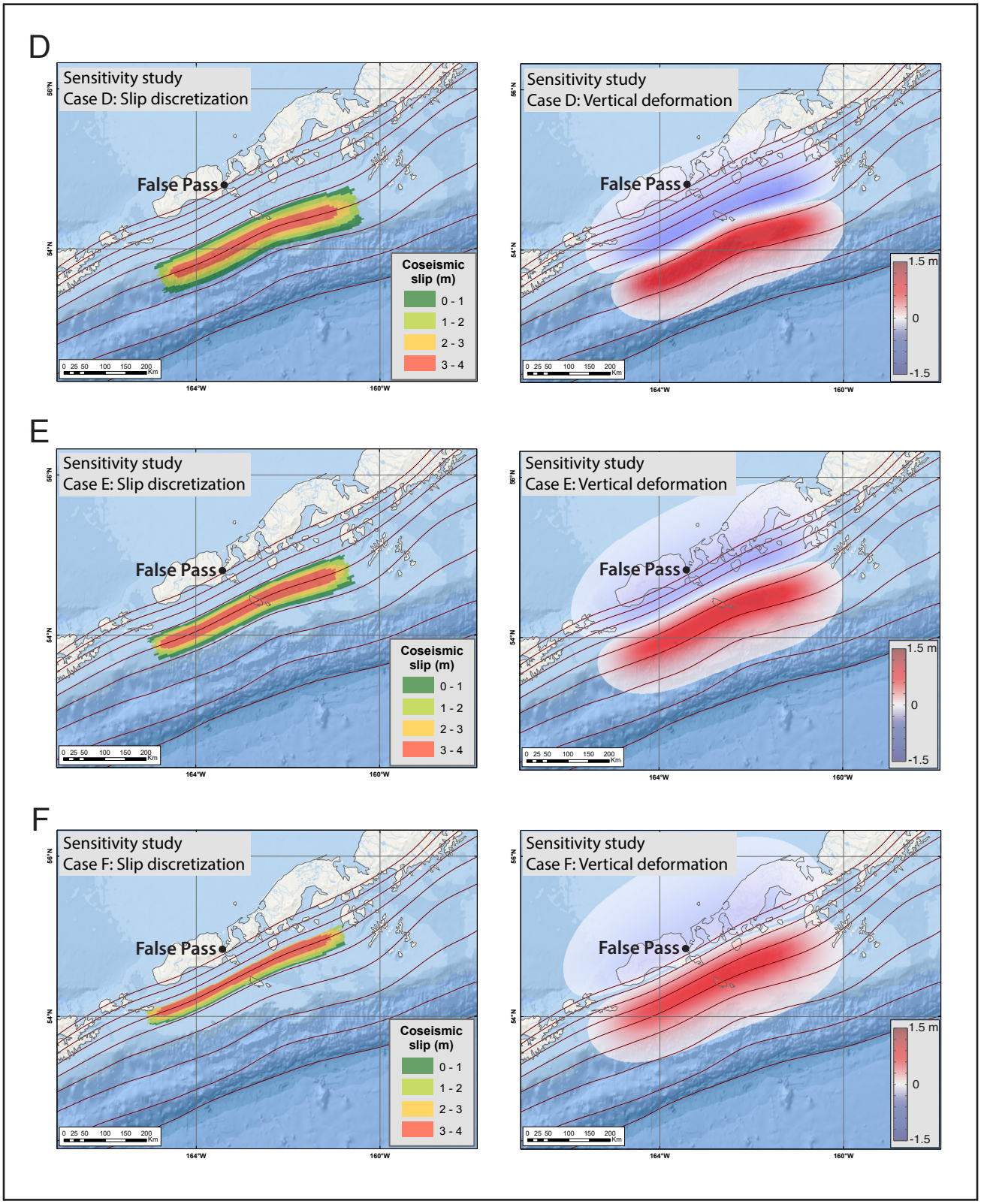

Figure 5, cont. Imposed slip distributions along the plate interface (left) and computed vertical ground surface deformations (right) for sensitivity cases D–F, modeling M_W 8.0 ruptures near False Pass. The slip location varies in the downdip direction of the plate interface while preserving the same slip patch configuration. Brown lines are depth contours of the subduction interface from 0 to 80 km with a 10-km interval.

Simulated water levels in False Pass vary considerably according to different earthquake slip distributions (fig. 6). The time series indicate that the ruptures at 30 km (18.6 mi) depth (case D) result in the highest wave amplitude in all locations, followed by cases C, the rupture at a depth of 20 km (12.4 mi), and B, the rupture at a depth of 10 km (6.2 mi). The shallow surface-breaching rupture represented by case A produces the smallest waves. Based on these results, we develop hypothetical ruptures with maximum slip in the 20–40 km (12.4–24.8 mi) depth range (cases C–D). As in Nicolsky and others (2016), we develop maximum credible scenarios by allowing up to 35 m (115 ft) of slip in the deep and intermediate sections of the Alaska–Aleutian megathrust and up to 50 m (164 ft) in the shallow sections of the megathrust. The maximum slip is imposed along regions of the megathrust that have the capability to generate the highest amplitude waves in False Pass.

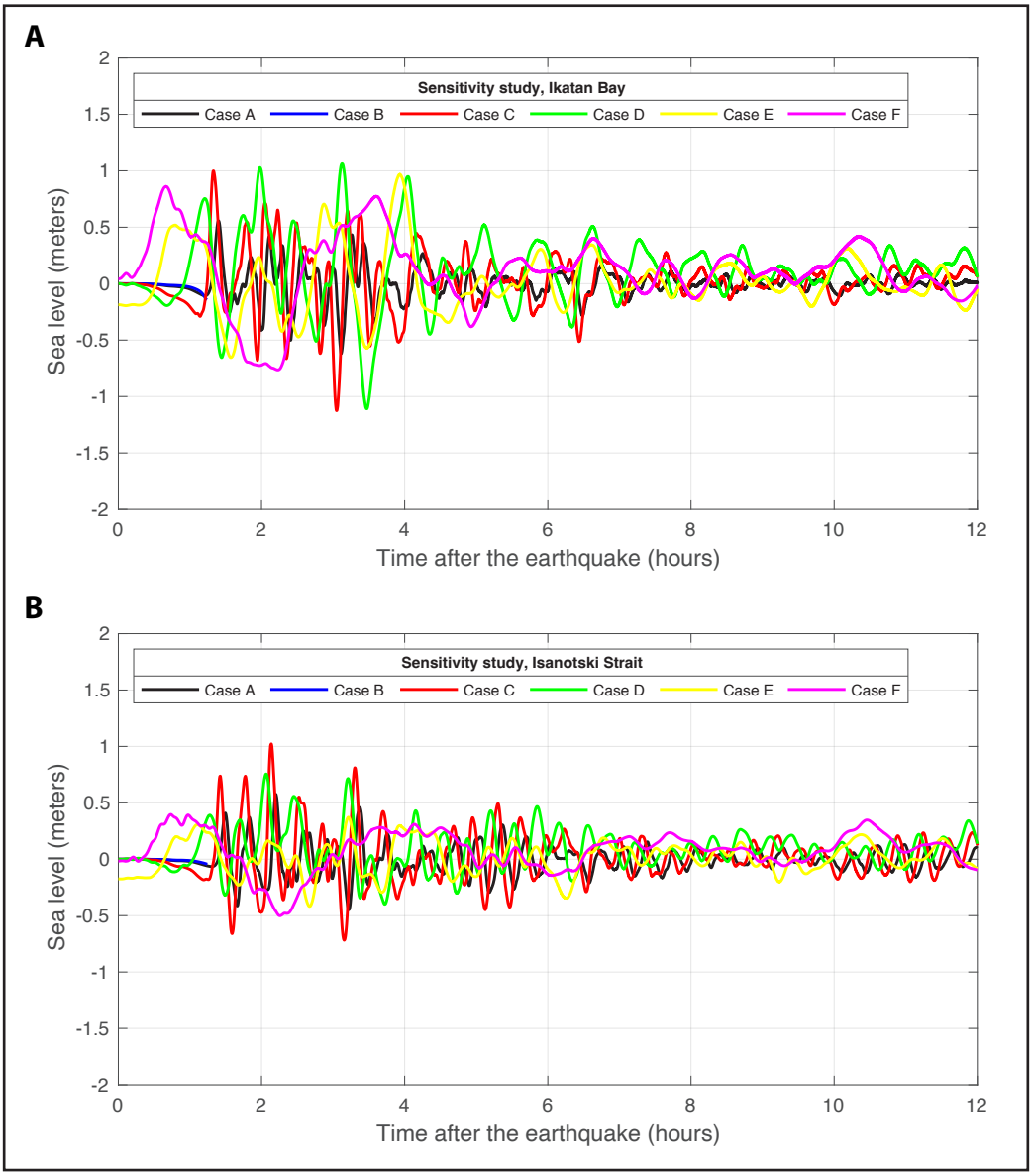

Figure 6. Modeled water-level dynamics (from the point of view of an observer standing at the shore) in (**A**) Ikatan Bay and (**B**) Isanotski Strait, for the ground surface deformations shown in figure 5. Model duration is 12 hours. The zero value of sea level corresponds to the post-earthquake MHHW level.

Hypothetical Tsunami Sources

In this section, we describe tsunamigenic Alaska–Aleutian megathrust earthquakes used for assessing tsunami hazard in False Pass (table 2). Our goal is to determine geologically plausible scenarios that will result in maximum reasonable tsunami inundation in the community, that is, credible worst-case scenarios. Scenarios are grouped according to their locations and specific source characterization.

Group I includes four scenarios that are based on results of the sensitivity study. Group II includes six scenarios that reflect the presence of Shumagin seismic gap as a freely slipping segment of the plate interface, and therefore do not have any earthquake slip placed in the gap region. Scenarios in Group III are developed under the assumption that the geodetic data are not representative of the long term; therefore the Shumagin seismic gap area can be included in a hypothetical rupture. We build scenarios in Group IV considering implications of the 2011 Tohoku earthquake (Wang and others, 2018), which assume that the maximum slip near the trench could be up to 50 m (164 ft). To be consistent with previous reports (e.g., Nicolsky and others, 2016, 2017; Suleimani and others, 2016), we consider scenarios with slip parameterization like that proposed by Butler and others (2014). Finally, Group V consists of a single scenario, which models a rupture of the Cascadia subduction zone as an example of a distant tsunami source.

In all scenarios, we do not account for the finite speed of rupture propagation along the fault, and we consider the ocean-bottom displacements to be instantaneous. All proposed scenarios are summarized in table 2. The proposed slip distributions and vertical coseismic deformations are shown in figure 7. We consider various downdip locations for the maximum slip to parameterize credible tsunamigenic earthquakes. In the downdip direction, the slip is determined by the slip skewness parameter q in the Freund and Barnett (1976) formulae. The average and maximum slip as well as the rupture areas are set according to the scaling relations of Papazachos and others (2005) and Moss and Travasarou (2006). We note that the presented tsunami sources are intended to capture the maximum credible scenarios and to provide a starting point for development of more complex models.

Group I

Scenarios in this group are based on the results of the sensitivity study. The proposed slip distributions and vertical coseismic deformations for scenarios 1–4 are shown in figure 7A–D.

Scenario 1: M_W 8.8 in the WAP region: maximum slip at a depth of 18–32 km (11.2–19.8 mi).	The depth of maximum slip corresponds to that of the combination of sensitivity cases C and D. The slip skewness parameter, q, is set to 0.5 (bell-shaped curve is centered) to model the patch of 35 m (115 ft) maximum slip centered at a depth of 25 km (15.5 mi).
Scenario 2: M_W 8.9 earthquake in the WAP region: maximum slip at a depth of 18–42 km (11.2–26.1 mi).	The depth of maximum slip corresponds to that of the combination of sensitivity cases C, D, and E. The slip skewness parameter, q, is set to 0.5 (bell-shaped curve is centered) to model the patch of 35 m (115 ft) maximum slip centered at a depth of 30 km (18.6 mi).

Table 2. The hypothetical megathrust scenarios used to model tsunami runup in False Pass (WAP = western Alaska Peninsula). Asterisk indicates scenarios that have been considered in previous inundation mapping reports.

Group	#	M_W	Description	Depth range km (mi)	Maximum slip depth range km (mi)	Maximum slip m (ft)	Ground subsidence in False Pass m (ft)
I	1	8.8	Earthquake in the WAP region with maximum slip at a depth of 15–35 km	10–40 (6.2–24.8)	18–32 (11.2–19.8)	35 (114.8)	0.86 (2.8)
	2	8.9	Earthquake in the WAP region with maximum slip at a depth of 15–45 km	10–50 (6.2–31.0)	18–42 (11.2–26.1)	35 (114.8)	2 (6.6)
	3	8.8	Earthquake in the WAP region with maximum slip at a depth of 25–45 km	20–50 (12.4–31.0)	28–42 (17.4–26.1)	35 (114.8)	1.8 (5.9)
	4	8.7	Earthquake in the WAP region with maximum slip at a depth of 35–55 km	30–60 (18.6–37.2)	38–52 (23.6–32.3)	35 (114.8)	1.7 (5.6)
II	5*	8.8	Earthquake in the WAP region: Eastern asperity only	5–45 (3.1–27.9)	10–30 (6.2–16.6)	15 (49.2)	0
	6*	8.9	Earthquake in the WAP region: Eastern asperity and trench	5–45 (3.1–27.9)	10–20 (6.2–12.4)	50 (164)	0
	7*	8.9	Earthquake in the WAP region: Western asperity only	5–35 (3.1–21.7)	13–17 (8.1–10.6)	9.9 (32.5)	0
	8*	8.9	Earthquake in the WAP region: Western asperity and trench	5–45 (3.1–27.9)	10–20 (6.2–12.4)	50 (164)	0.24 (0.79)
	9*	9.0	Earthquake in the WAP region: Two asperities and trench	5–35 (3.1–21.7)	10–20 (6.2–12.4)	50 (164)	0.13 (0.43)
	10*	9.0	Earthquake in the WAP region: Two asperities, weakly connected	5–45 (3.1–27.9)	10–20 (6.2–12.4)	50 (164)	0.29 (0.95)
III	11*	9.0	Earthquake in the WAP region: Predominantly shallow slip in the western part of the rupture	5–45 (3.1–27.9)	5–15 (3.1–9.3)	50 (164)	0.8 (2.62)
	12*	9.1	Earthquake in the WAP region: Predominantly shallow slip in the eastern part of the rupture	5–45 (3.1–27.9)	5–15 (3.1–9.3)	50 (164)	0.6 (1.97)
	13*	8.8	Earthquake in the WAP region: Gap-filling event with shallow slip	2–28 (1.2–17.4)	5–15 (3.1–9.3)	50 (164)	0.05 (0.16)
IV	14*	9.2	Earthquake in the WAP region with uniform along-strike maximum slip at a depth of 12-20 km	5–50 (3.1–31.0)	12–20 (7.5–12.4)	36.6 (120.0)	1.58 (5.2)
	15*	9.25	Earthquake in the WAP region with uniform along-strike maximum slip at a depth of 5-20 km	5–30 (3.1–18.6)	5–20 (3.1–12.4)	50 (164.0)	0.26 (0.85)
	16*	9.3	Earthquake in the WAP region: 50 m of maximum slip close to the trench	2–30 (1.2–18.6)	0.5 – 18 (0.3–11.2)	50 (164.0)	0.31 (1)
	17*	9.3	Earthquake in the WAP region: 35 m of maximum slip across the majority of the rupture	2–38 (1.2–23.6)	7–32 (4.3–19.8)	35.0 (115.0)	1.15 (3.8)
V	18*	9.1	Earthquake in the Cascadia subduction zone (Wang and others, 2003)	?	?	45.0 (148.0)	0

Scenario 3: M_W 8.8 earthquake in the WAP region: maximum slip at a depth of 28–42 km (17.4–26.1 mi).	The depth of maximum slip corresponds to that of the combination of sensitivity cases D and E. The slip skewness parameter, q, is set to 0.5 (bell-shaped curve is centered) to model the patch of 35 m (115 ft) maximum slip centered at a depth of 35 km (21.7 mi).
Scenario 4: M_W 8.7 earthquake in the WAP region: maximum slip at a depth of 38–52 km (23.6–32.3 mi).	The depth of maximum slip corresponds to that of the combination of sensitivity cases E and F. The slip skewness parameter, q, is set to 0.5 (bell-shaped curve is centered) to model the patch of 35 m (115 ft) maximum slip centered at a depth of 45 km (27.9 mi).

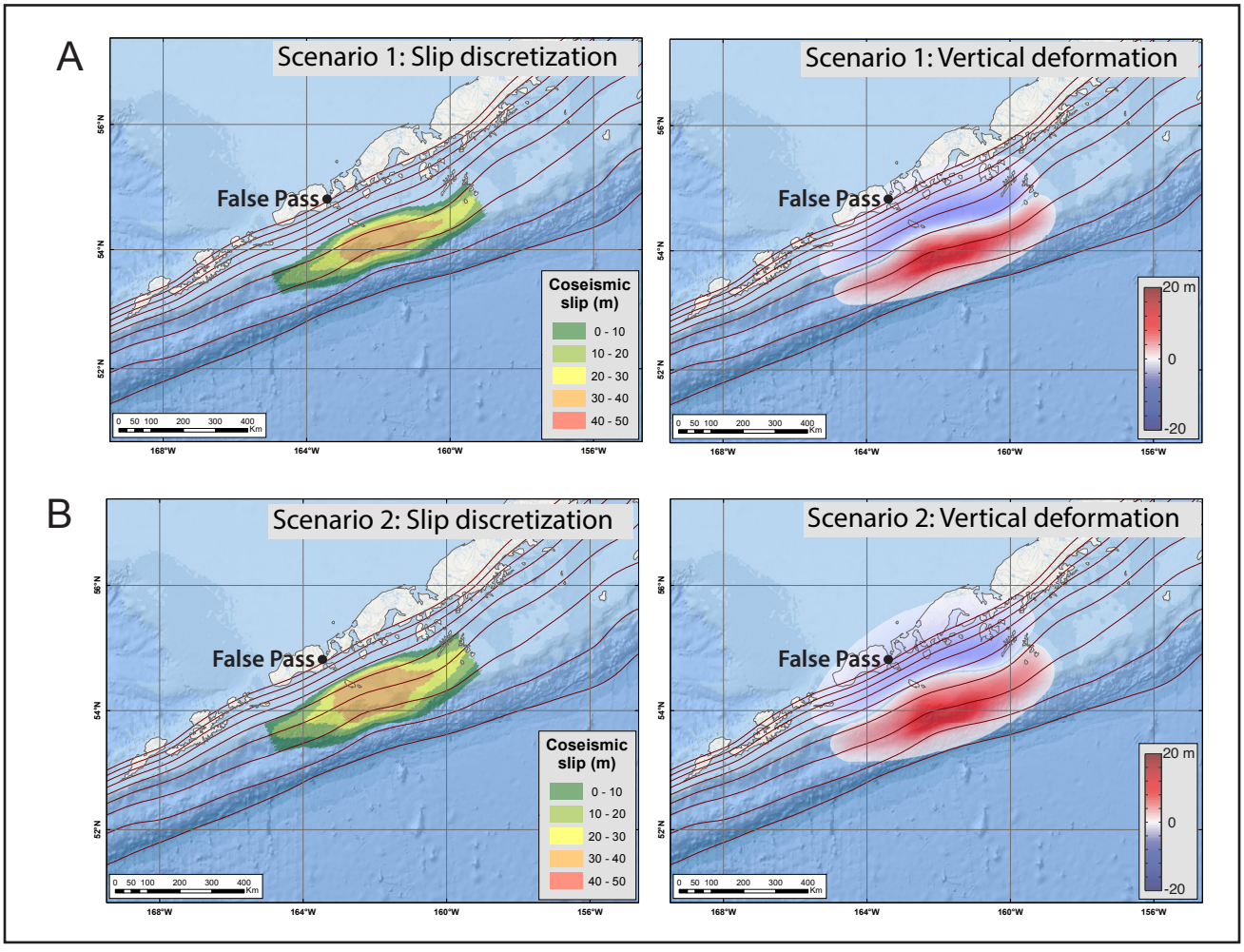

Figure 7. Estimated slip distribution along the plate interface (left) for scenarios 1–2 and computed vertical ground surface deformation (right) for scenarios 1–2. Brown lines are depth contours of the subduction interface from 0 to 80 km with a 10-km interval.

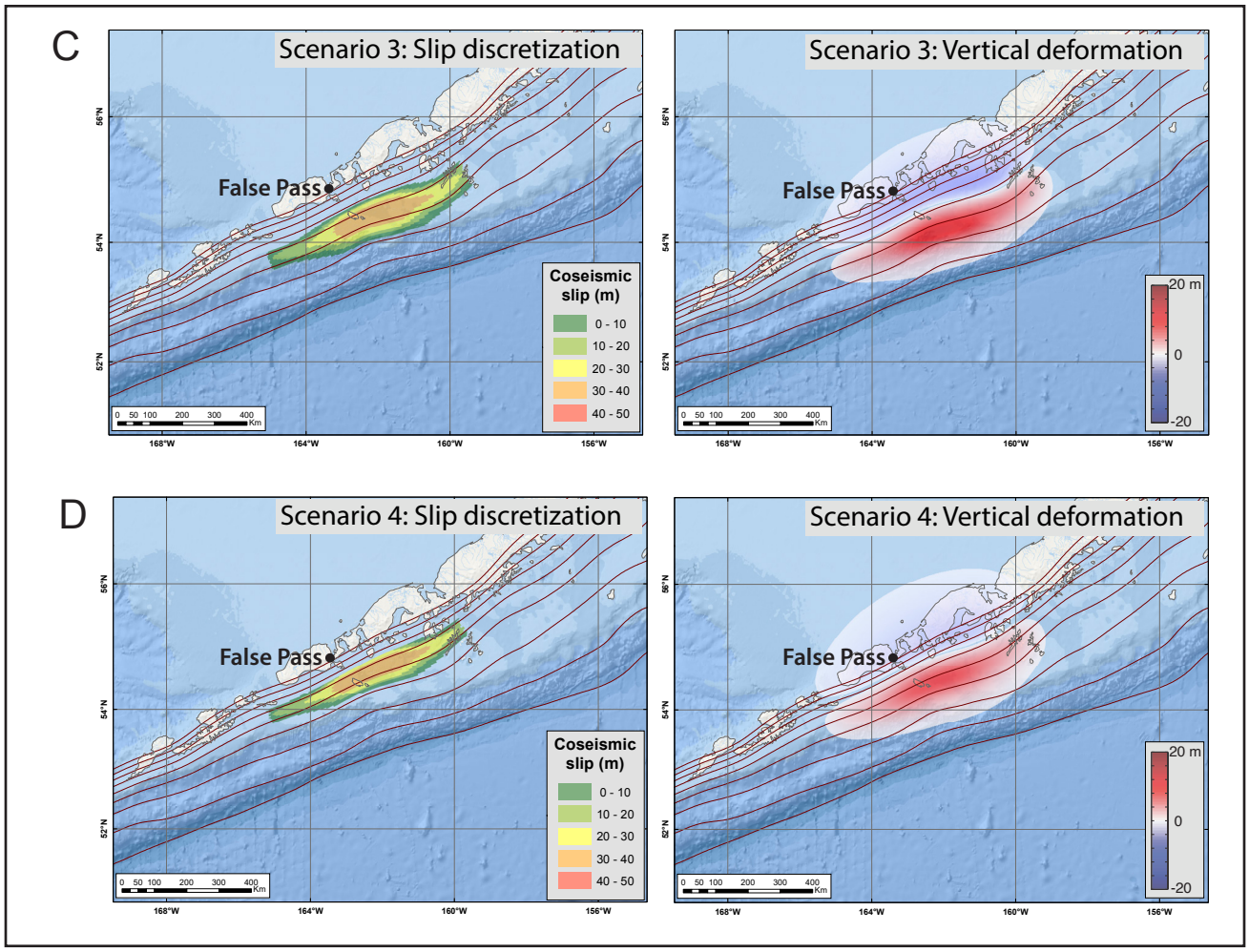

Figure 7, cont. Estimated slip distribution along the plate interface (left) for scenarios 3–4 and computed vertical ground surface deformation (right) for scenarios 3–4. Brown lines are depth contours of the subduction interface from 0 to 80 km with a 10-km interval.

Group II

Scenarios in this group have been considered previously in the tsunami inundation mapping study of the communities King Cove and Cold Bay on the WAP (Suleimani and others, 2016). Since False Pass is in the same region of the subduction zone, these scenarios can be utilized in the current numerical modeling study. They are potential M_W 8.6–9.0 earthquakes that reflect the presence of Shumagin seismic gap as a freely slipping segment of the plate interface, and therefore do not have any slip placed in the gap region. Refer to Suleimani and others (2016) for detailed description of the methodology used to constrain slip distributions in scenarios 5–10.

The proposed slip distributions and vertical coseismic deformations for scenarios 5–10 are shown in figure 7E–J.

Scenario 5: M_W 8.8 earthquake in the WAP region: Eastern asperity only.

This is scenario 5 in Suleimani and others (2016). The source consists of an eastern asperity with the maximum slip of 15 m (49.2 ft) at a depth of 10–30 km (6.2–16.6 mi).

Scenario 6: M_W 8.9 earthquake in the WAP region: Eastern asperity and trench.	This is scenario 3 in Suleimani and others (2016). The source consists of an eastern asperity, and an area of higher slip at the shallow depth, close to the trench. The maximum slip of 50 m (164 ft) is at a depth of 10–20 km (6.2–12.4 mi).
Scenario 7: M_W 8.9 earthquake in the WAP region: Western asperity only.	This is scenario 6 in Suleimani and others (2016). The source consists of a western asperity only with the maximum slip of 9.9 m (32.5 ft) at a depth of 13–17 km (8.1–10.6 mi).
Scenario 8: M_W 8.9 earthquake in the WAP region: Western asperity and trench.	This is scenario 4 in Suleimani and others (2016). The source consists of a western asperity, and an area of higher slip at the shallow depth, close to the trench. The maximum slip of 50 m (164 ft) is at a depth of 10–20 km (6.2–12.4 mi).
Scenario 9: M_W 9.0 earthquake in the WAP region: Two asperities and trench.	This is scenario 1 in Suleimani and others (2016). The source consists of a western and eastern asperity, separated by the Shumagin seismic gap and connected only by slip in the shallow part of the rupture, close to the trench. The maximum slip of 50 m (164 ft) is at a depth of 10–20 km (6.2–12.4 mi).
Scenario 10: M_W 9.0 earthquake in the WAP region: two asperities, weakly connected.	This is scenario 2 in Suleimani and others (2016). The source consists of a western and eastern asperity, separated by the Shumagin seismic gap and connected only by slip in the shallow part of the rupture, close to the trench. The difference between this scenario and scenario 9 is in the amount of slip placed in the area connecting the two asperities, which is much smaller in this scenario. The maximum slip of 50 m (164 ft) is at a depth of 10–20 km (6.2–12.4 mi).

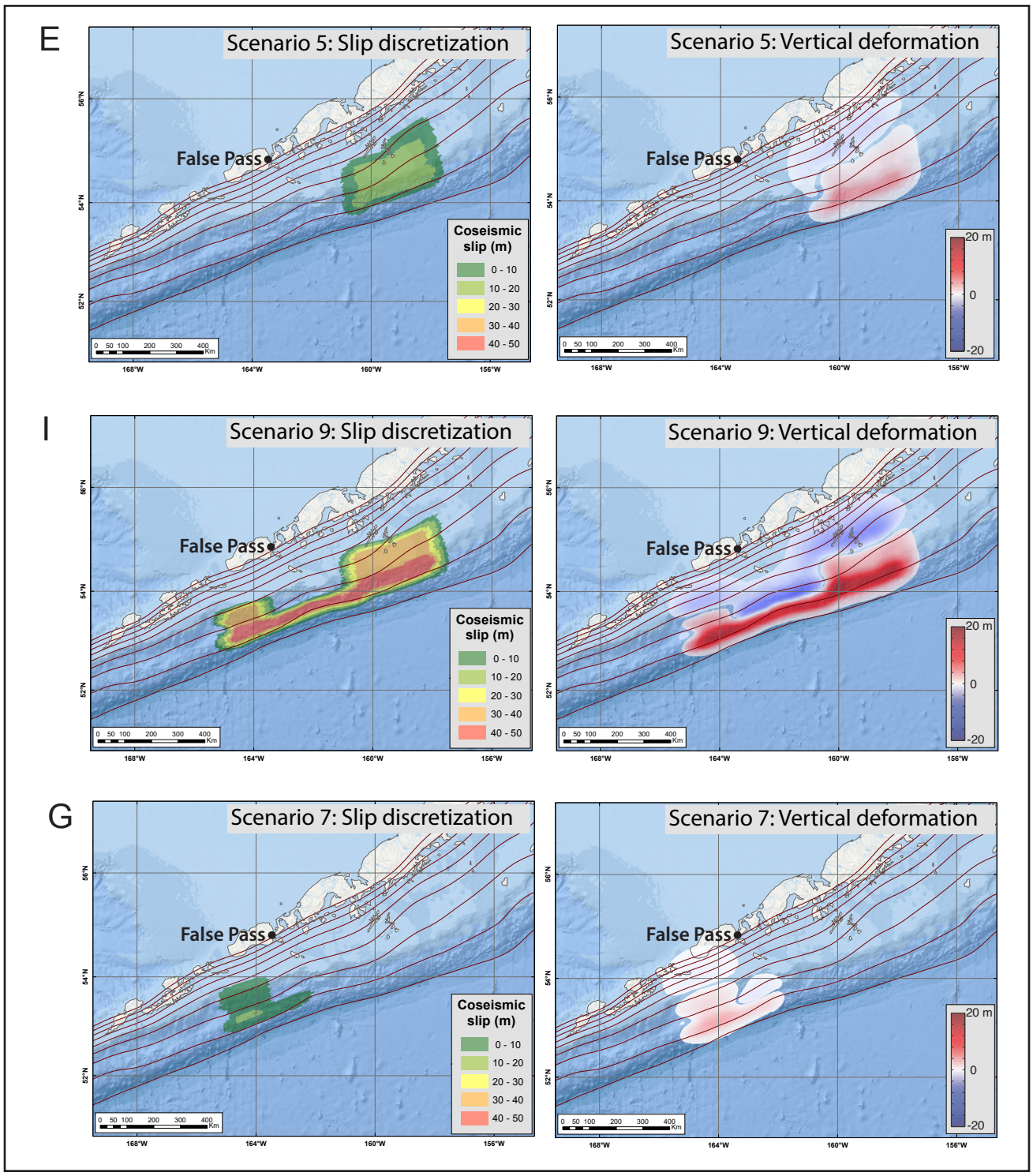

Figure 7, cont. Estimated slip distribution along the plate interface (left) for scenarios 5–7 and computed vertical ground surface deformation (right) for scenarios 5–7. Brown lines are depth contours of the subduction interface from 0 to 80 km with a 10-km interval.

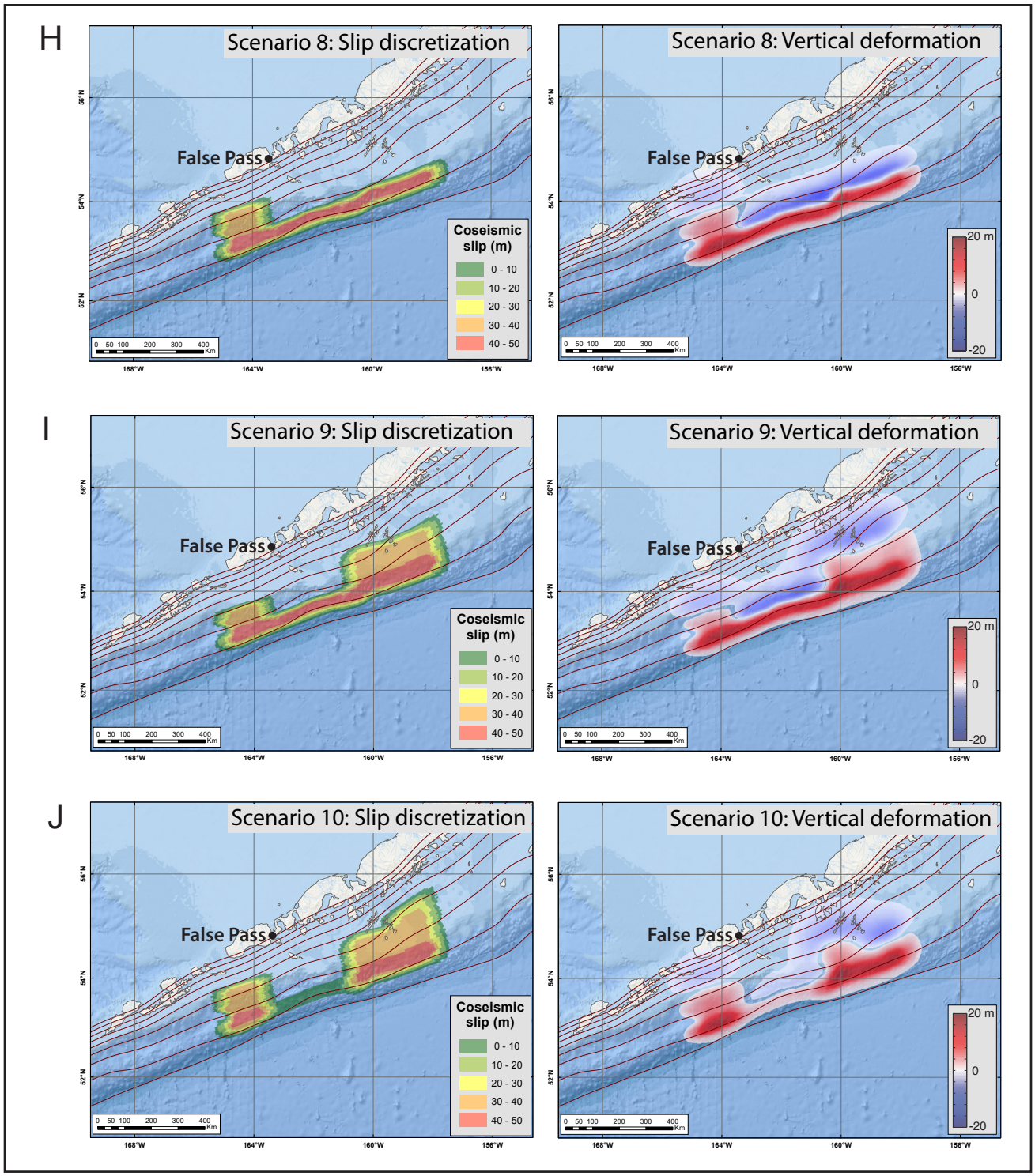

Figure 7, cont. Estimated slip distribution along the plate interface (left) for scenarios 8–10 and computed vertical ground surface deformation (right) for scenarios 8–10. Brown lines are depth contours of the subduction interface from 0 to 80 km with a 10-km interval.

Group III

Scenarios in this group have also been considered previously in the tsunami inundation mapping study of the communities King Cove and Cold Bay on the WAP (Suleimani and others, 2016). They are potential M_W 8.8–9.0 earthquakes developed under the assumption that the geodetic data are not representative of the long term, and therefore the Shumagin seismic gap area can be included in a hypothetical rupture. The objective here is not to limit our assessment of future tsunami hazards by using only historically observed slip patterns and geodetic models. For the scenarios in this group, we assume that the presence of Shumagin gap has no effect on the current degree of plate locking or accumulated slip deficit in the WAP region. This approach allows us to determine whether the inclusion of slip in the gap segment in deformation models will result in run-up values in False Pass comparable to that from source models that are constrained by geodetic and geologic data. At the same time, we are assessing the tsunami impact from earthquakes of lower magnitudes that have potentially shorter recurrence intervals. Refer to Suleimani and others (2016) for a detailed description of the methodology used to constrain slip distributions in scenarios 11–13.

The proposed slip distributions and vertical coseismic deformations for scenarios 11–13 are shown in figure 7K–M.

Scenario 11: M_W 9.0 earthquake in the WAP region: Predominantly shallow slip in the western part of the rupture.

This is scenario 8 in Suleimani and others (2016). The source consists of a western asperity that is spread downdip between 5 and 45 km (3.1–28 mi) depth, and a narrow segment in the eastern part of the rupture at a depth of 20–40 km (12–25 mi). In this scenario, the segments representing the Shumagin seismic gap have non-zero slip. The western asperity has the maximum slip of 50 m (164 ft) at a depth of 5–15 km (3–9 mi), close to the trench, and in the rest of the rupture the maximum slip is 38 m (125 ft).

Scenario 12: M_W 9.1 earthquake in the WAP region: Predominantly shallow slip in the eastern part of the rupture.

This is scenario 9 in Suleimani and others (2016). The source consists of an eastern asperity that is spread downdip between 5 and 45 km (3.1–28 mi) depth, and a narrow segment in the western part of the rupture at a depth of 30–45 km (18.6–28 mi). In this scenario, the segments representing the Shumagin seismic gap have non-zero slip. The eastern asperity has the maximum slip of 50 m (164 ft) at a depth of 5–15 km (3–9 mi) close to the trench, and in the rest of the rupture the maximum slip is 37 m (121 ft).

Scenario 13: M_W 8.8 earthquake in the WAP region: Gap-filling event with shallow slip.

This is scenario 7 in Suleimani and others (2016). In this scenario, the segments representing the Shumagin gap have non-zero slip. The source consists of a patch with maximum slip of 50 m (164 ft) at a depth of 5–15 km (3–9 mi), and in the rest of the rupture area the maximum slip is 37 m (121 ft).

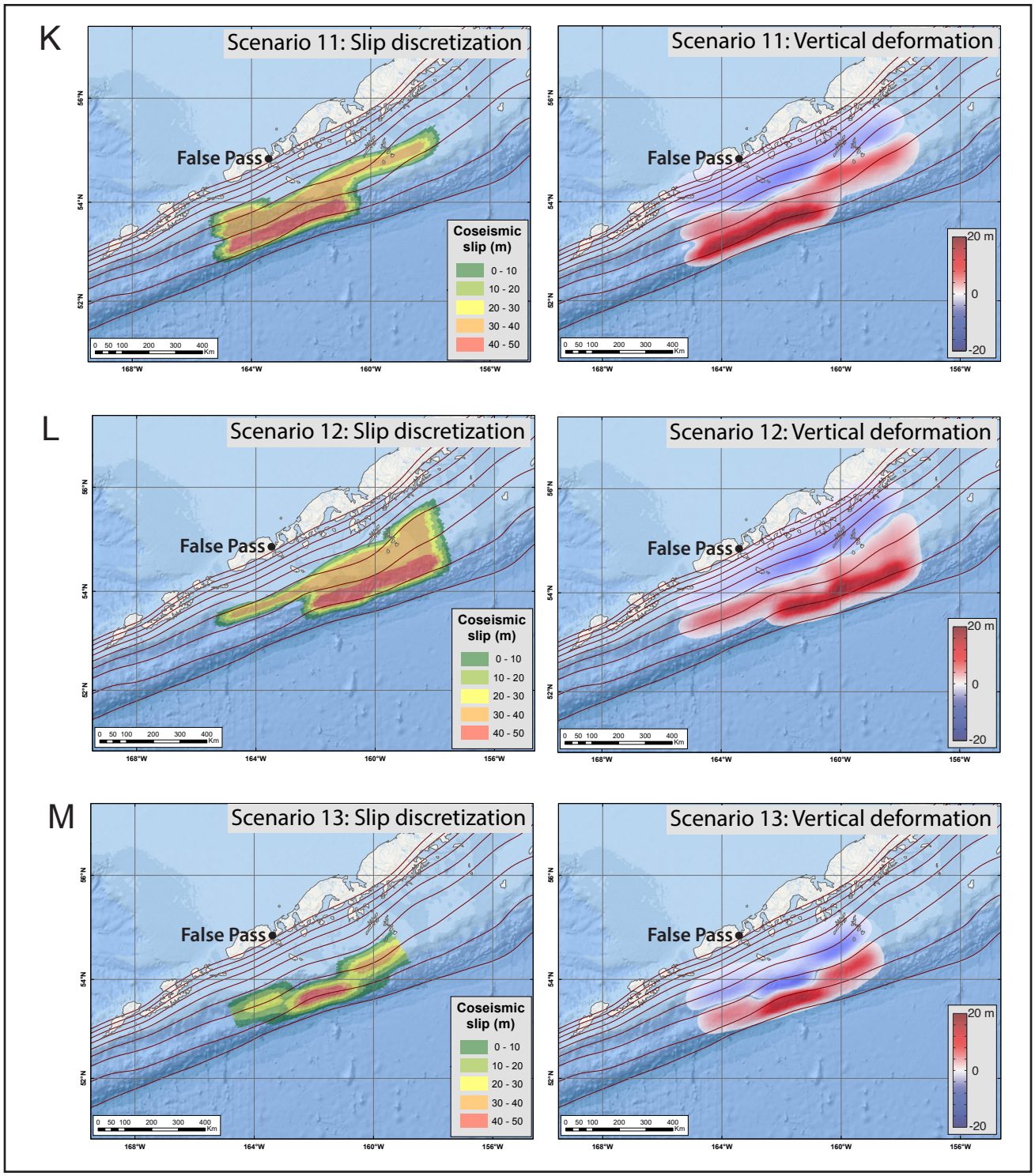

Figure 7, cont. Estimated slip distribution along the plate interface (left) for scenarios 11–13 and computed vertical ground surface deformation (right) for scenarios 11–13. Brown lines are depth contours of the subduction interface from 0 to 80 km with a 10-km interval.

Group IV

Ryan and others (2012), and later Kirby and others (2013), compared the Alaska and Tohoku margins and suggested that a hypothetical rupture in the Alaska–Aleutian subduction zone might propagate to shallow depths as it did in the M_W 9.0 Tohoku earthquake. Shallow fault rupture at the Tohoku margin resulted in a complex mix of blind (concealed) fault-bend folding along the fault length and surface-breaching rupture of the seafloor—both of which contributed to a significant seafloor disturbance. Multibeam bathymetry in the eastern part of the Aleutian megathrust suggests that the Alaska plate margin has similar mixed-behavior shallow ruptures.

Recently, Butler and others (2014) described a layer of sand discovered in the Makauwahi sinkhole on the island of Kaua'i, Hawai'i. The origin of this layer was presumed to be the inundation of the sinkhole by a giant paleotsunami following a M_W 9+ earthquake in the eastern Aleutian Islands. Butler (2012) provides an in-depth examination of previous great Aleutian earthquakes and tsunamis impacting Hawai'i. In subsequent research, Butler (2014) considered several hypothetical events with a 35 m (114.8 ft) displacement on the megathrust and up to a 50 m (164 ft) displacement near the trench.

Scenarios 14–17 simulate hypothetical ruptures in the eastern part of the Alaska–Aleutian megathrust where the updip and downdip limits of the rupture are between 0 km and 30–50 km (18.6–24.8 mi). However, we account for the possibility that the slip in the earthquake rupture may be concentrated at the shallowest depths of the plate interface and may breach the sea floor at the trench. We construct scenario 16 with modeled fault slip extending to the shallowest part of the megathrust. In all scenarios, the slip is distributed uniformly along strike. The proposed slip distributions and vertical coseismic deformations for scenarios 14–17 are shown in figures 7N–Q.

Scenario 14: M_W 9.2 earthquake in the WAP region with uniform along-strike maximum slip at a depth of 12-20 km.

The depth of maximum slip corresponds to that of the combination of sensitivity cases B and C. The slip skewness parameter, q, is set to 0.25 (bell-shaped curve skewed toward the trench) to model the maximum slip of 36.6 m (120 ft) at a depth of 15 km (9.3 mi), and 25 m (82 ft) in the rest of the rupture.

Scenario 15: M_W 9.25 earthquake in the WAP region with uniform along-strike maximum slip at a depth of 5–20 km.

This is scenario 11 in Suleimani and others (2016). In this scenario we assume a 20 m (65 ft) slip on the plate interface between the 20 km (12.4 mi) and 30 km (18.6 mi) depth, and up to a 50 m (164 ft) slip between the depths of 5 km (1.2 mi) and 20 km (12.4 mi) depth.

Scenario 16: M_W 9.3 earthquake in the WAP region: 50 m of maximum slip close to the trench.

In this scenario similar to Butler (2014) we assume a 20 m (65 ft) slip on the plate interface between the 18 km (11.2 mi) and 30 km (18.6 mi) depth, and up to a 50 m (164 ft) slip near the trench, that is, between 0.5 km (0.3 mi) and 18 km (11.2 mi) depth. According to the USGS letter (Butler, 2014; app. 2), this so-called 50/20 slip model "is starting to approach that more realistic model" that could occur in the Aleutian Islands.

Scenario 17: M_W 9.3 earthquake in the WAP region: 35 m of maximum slip across the majority of the rupture.

In this scenario, like Butler (2014), we assume 35 m (114.8 ft) of slip for nearly the entire rupture patch between the 7 km (4.3 mi) and 32 km (19.8 mi) depth contours, with slip decreasing both toward the trench and to the deeper parts of the rupture. A similar scenario was proposed in the tsunami modeling study for Kodiak Island (scenario 8 of Suleimani and others, 2017).

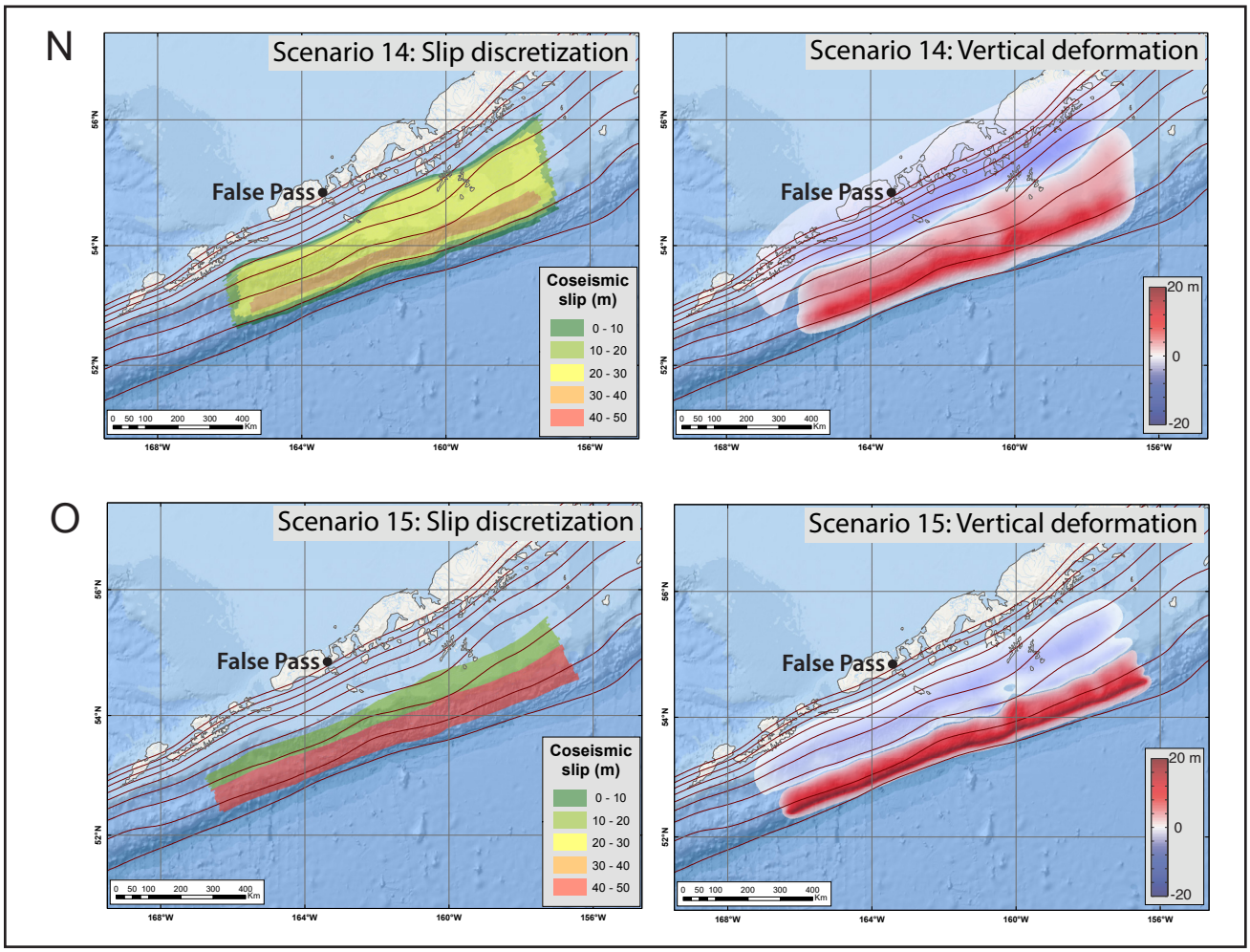

Figure 7, cont. Estimated slip distribution along the plate interface (left) for scenarios 14–15 and computed vertical ground surface deformation (right) for scenarios 14–15. Brown lines are depth contours of the subduction interface from 0 to 80 km with a 10-km interval.

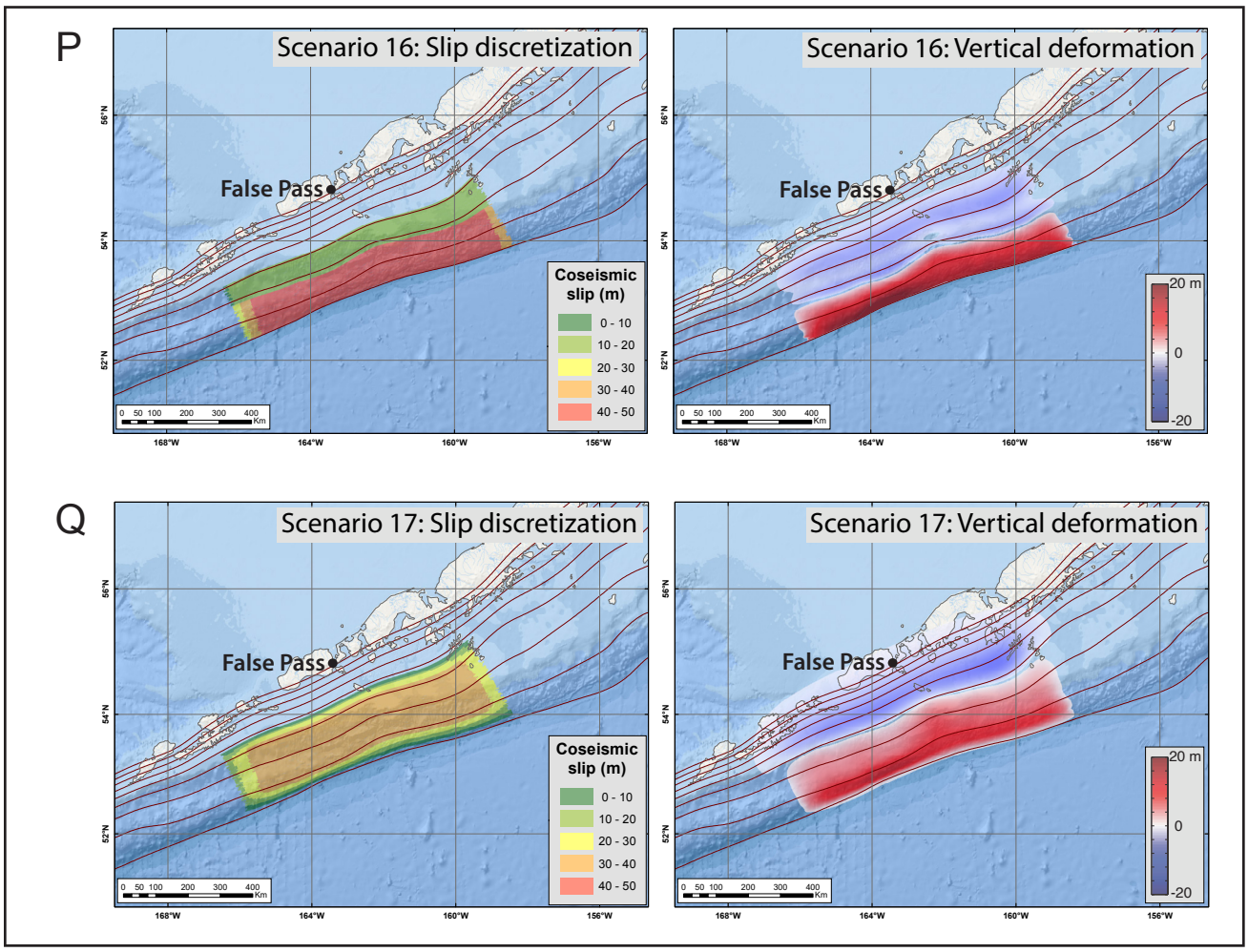

Figure 7, cont. Estimated slip distribution along the plate interface (left) for scenarios 16–17 and computed vertical ground surface deformation (right) for scenarios 16–17. Brown lines are depth contours of the subduction interface from 0 to 80 km with a 10-km interval.

Group V

Scenario 18: Rupture of the Cascadia subduction zone, including the entire megathrust between British Columbia and northern California

Scenario 18 considers a hypothetical tsunami generated along the coast of the Pacific Northwest US—relatively distant from Unimak Island. Although a rupture of the Cascadia subduction zone is not a worst-case scenario for False pass, this scenario is included for the sake of community preparedness. This scenario is the same as scenario 16 in the tsunami modeling studies for King Cove and Cold Bay (Suleimani and others, 2016). The slip distribution model for this scenario is shown in figure 10 of Wang and others (2003). The vertical coseismic deformations for scenario 16 are shown in figure 7R.

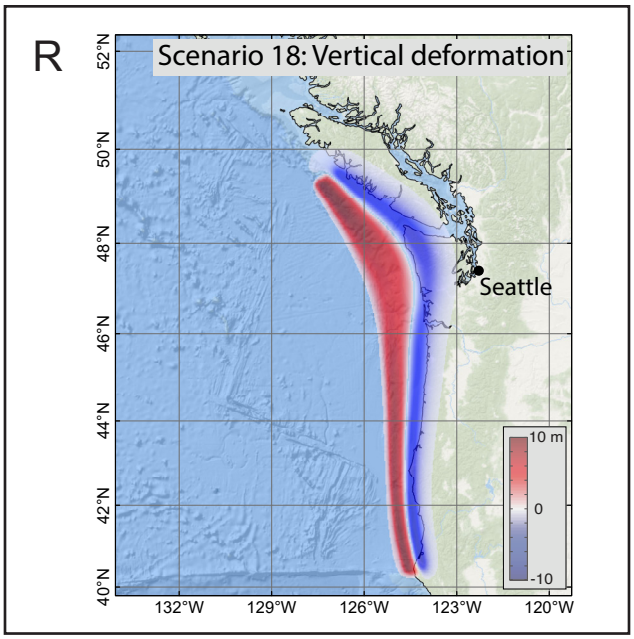

Figure 7, cont. Computed vertical ground surface deformation for scenario 18 (slip distribution is not provided for scenario 18).

MODELING RESULTS

We modeled water dynamics for each of the previously described scenarios summarized in table 2. The extent of inundation and flow depths were calculated only for the level 4 high-resolution grid. The map sheet shows the maximum composite extent of inundation for all scenarios, and the maximum composite flow depths over dry land. Refer to the "Grid Development and Data Sources" section of this report for a description of how the composite flow depth maps and the composite tsunami inundation lines are generated from multiple scenarios. The calculated extent of inundation accounts for regional coseismic deformation in False Pass.

First, we analyze the extent of tsunami inundation for all scenarios, organizing them by scenario groups. Then we select the scenario in each group that results in the largest inundation zone and plot the corresponding inundation lines (fig. 8). Scenario 11 from Group III results in the worst overall inundation. It is followed by scenarios 17 from Group IV, scenario 2 from Group I, and scenario 9 from Group II. Because these scenarios are from different groups, it demonstrates that sizable tsunami effects could be produced by coseismic slip at different depths of the subduction interface. Scenario 18, the megathrust earthquake in the Cascadia subduction zone, resulted in the least amount of inundation. Scenarios 2, 11, and 17 result in the largest inundation zones and therefore have a sizable contribution to the composite inundation map (map sheet 1).

Time Series

The arrival time of the first wave, the maximum wave amplitude, and the duration of wave action are all important factors that should be considered by emergency managers during evacuation planning. Therefore, we supplement the inundation maps with time series of modeled water level and velocity dynamics at certain locations around False Pass. Appendix A contains plots of sea level and velocity time series for selected scenarios. These selected scenarios are those that result in maximum inundation in each scenario group for a community. For each location—shown by a number in figure A1, we plot the sea level and water velocity in figure A2.

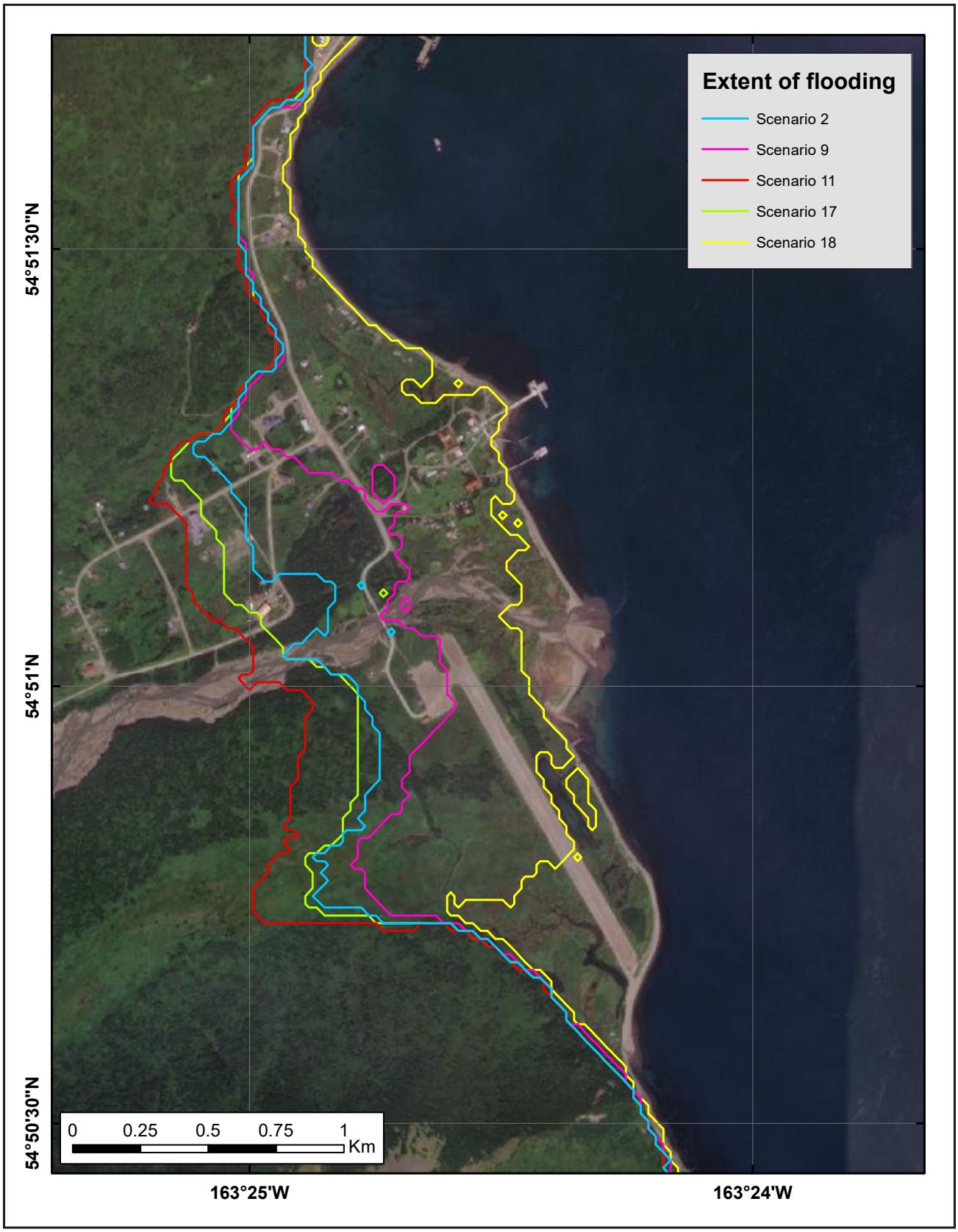

Figure 8. Tsunami inundation in False Pass for the worst-case scenarios from each scenario group.

In all plots in appendix A, zero time corresponds to the time at which the earthquake occurs. The pre-earthquake elevation/depth with respect to the MHHW is stated for each location. The post-earthquake elevation/depth corresponding to the MHHW datum is also listed for each scenario in table A1. To show the height of arriving tsunamis for offshore locations we use a vertical datum with a zero-mark corresponding to the pre-earthquake sea level. Velocity was computed only where the water depth is greater than 0.3 m (1.0 ft). The velocity magnitude is calculated as water flux divided by water depth; thus, the uncertainty can be large when the water depth is small.

The maximum water level values for all considered scenarios are listed in table A2, and maximum velocity values are given in table A3.

SOURCES OF ERRORS AND UNCERTAINTIES

The hydrodynamic model used to calculate propagation and run-up of tectonic tsunamis is a nonlinear, flux-formulated, shallow-water model (Nicolsky and others, 2011b) that passed the verification and validation tests required for numerical codes used to produce tsunami inundation maps (Synolakis and others, 2007; NTHMP, 2012). The spatial resolution of the grid used to calculate tsunami inundation in False Pass is about 14 m (46 ft) and satisfies NOAA minimum recommended requirements for computation of tsunami inundation (NTHMP, 2010). Although this resolution is high enough to describe major relief features, small topographic features, buildings, and other facilities cannot be resolved accurately by the existing model. We also note that uncertainty in grid-cell elevation/depth propagates into the modeling results and eventually contributes to horizontal uncertainty in the location of the inundation line.

Another contribution to this uncertainty is the paucity of data in the intertidal zone. However, no established practices exist to directly propagate the digital elevation model uncertainty into the uncertainty of the inundation line (Hare and others, 2011). The direction of the incoming waves, their amplitudes, and times of arrival are primarily determined by displacements of the ocean in the source area. Therefore, the inundation modeling results for local sources are especially sensitive to the fine structure of the tsunami source. The modeling process is highly sensitive to errors when the complexity of the source function is combined with its proximity to the coastal zone.

Most of the errors/uncertainties in the numerical predictions originate from the tsunamigenic earthquake sources used in the numerical models. Our assessment of potential earthquake scenarios is not exhaustive and represents a best estimate of the locations and sizes of potential tsunami-generating events. It is possible that other unrecognized earthquake scenarios or slope failures (both subaerial and submarine) could present hazards to False Pass. However, the scenarios presented in this report are intended to cover the range of potential situations about which the communities should be aware.

SUMMARY

We present results of numerical modeling of earthquake-generated tsunamis for the community of False Pass. The hypothetical tsunamigenic earthquakes used in this report are considered worst-case, maximum-possible slip scenarios for the eastern end of the Alaska–Aleutian megathrust. Each scenario represents a unique set of carefully selected geologic conditions (including rupture location and the amount of slip on the plate interface), and while these events are plausible, we make no attempt to estimate the likelihood that these events may occur in the near or distant geologic future. Our goal is to identify potential hazards to the communities to reduce impacts in future worst-case events.

A hypothetical earthquake with maximum slip distributed between depths of 10 and 20 km (6.2 and 12.4 mi) results in “worst case” tsunami inundation in False Pass. The maximum predicted overland flow depths for low-lying coastal areas reach 10 m (32.8 ft) with currents as strong as 15

m/sec (29.2 knots). Dangerous wave activity is expected to last for at least 12 hours after the hypothetical worst-case earthquakes.

The map sheet, which shows the potential extent of inundation and the tsunami flow depths, has been compiled using the best information available and is believed to be accurate; however, its preparation required many assumptions. We considered several tsunami scenarios and have provided an estimate of maximum credible tsunami inundation. Actual conditions during a tsunami event may vary from those considered, so the accuracy of predictions based on the modeling presented in this report cannot be guaranteed. The limits of inundation shown should only be used as a guideline for emergency planning and response action. Actual inundated areas will depend on specifics of earthquake deformation, ongoing and future on-land and offshore construction, and tide level, and may differ from areas shown on the maps. The information on these maps is intended to assist state and local agencies in planning for emergency evacuation and tsunami response actions in the event of a major tsunamigenic earthquake. Because these earthquake scenarios do not incorporate probabilities of occurrence, the results are not intended for land-use regulation or building-code development.

ACKNOWLEDGMENTS

This report was funded by the U.S. Department of Commerce/National Oceanic and Atmospheric Administration (NOAA) through National Tsunami Hazard Mitigation Program Awards NA21NWS4670003 and NA22NWS4670012 to the Alaska Division of Homeland Security and Emergency Management. This does not constitute an endorsement by NOAA. Numerical calculations for this work were supported by High Performance Computing resources at the Research Computing Systems unit at the Geophysical Institute of the University of Alaska Fairbanks.

REFERENCES

Argus, D.F., Gordon, R.G., Heflin, M.B., Ma, Chopo, Eanes, R.J., Willis, Pascal, Peltier, W.R., and Owen, S.E, 2010, The angular velocities of the plates and the velocity of the Earth's centre from space geodesy: Geophysics Journal International, v. 180, no. 3, p. 913–960. https://doi.org/10.1111/j.1365-246X.2009.04463.x

Butler, Rhett, 2012, Re-examination of the potential for great earthquakes along the Aleutian island arc with implication for tsunamis in Hawai'i: Seismological Research Letters, v. 83, no. 1, p. 30–39. https://doi.org/10.1785/gssrl.83.1.29

———2014, Great Aleutian tsunamis: Honolulu, HI, University of Hawai'i at Manoa, Hawai'i Institute of Geophysics & Planetology, Peer-Reviewed Report HIGP-2014-1, 170 p.

Butler, Rhett, Burney, David, and Walsh, David, 2014, Paleo-tsunami evidence on Kaua'i and numerical modeling of a great Aleutian tsunami: Geophysical Research Letters, v. 41, no. 19, p. 6,795–6,802. https://doi.org/10.1002/2014GL061232

Department of Commerce, Community, and Economic Development (DCCED)/Division of Community and Regional Affairs (DCRA), 2015, Community Database Online. https://dcra-cdo-dcced.opendata.arcgis.com/

DeMets, Charles, Gordon, R.C., Argus, D.F., and Stein, Seth, 1990, Current plate motions: Geophysical Journal International, v. 101, no. 2, p. 425–478.

Dunbar, P.K., and Weaver, C.S., 2008, U.S. states and territories national tsunami hazard assessment—Historical record and sources for waves: Technical Report, National Oceanic and Atmospheric Administration and U.S. Geological Survey, 59 p. https://repository.library.noaa.gov/view/noaa/47448

Elliott, J.L., Grapenthin, Ronni, Parameswaran, R.M., Xiai, Zhuohui, Freymueller, J.T., and Fusso, Logan, 2022, Cascading rupture of a megathrust: Science Advances, v. 18, no. 18, 10 p. https://doi.org/10.1126/sciadv.abm4131

Freund, L.B., and Barnett, D.M., 1976, A two-dimensional analysis of surface deformation due to dip-slip faulting: Bulletin of the Seismological Society of America, v. 66, no. 3, p. 667–675.

Geist, E.L., and Parsons, Tom, 2006, Probabilistic analysis of tsunami hazards: Natural Hazards, v. 37, no. 3, p. 277–314. https://doi.org/10.1007/s11069-005-4646-z

Hare, Rob, Eakins, B.W., and Amanate, Christopher, 2011, Modelling bathymetric uncertainty: International Hydrographic Review, p. 31–42. https://journals.lib.unb.ca/index.php/ihr/article/view/20888

Hayes, Gavin, 2018, Slab2–A comprehensive subduction zone geometry model: U.S. Geological Survey data release. https://doi.org/10.5066/F7PV6JNV

Kirby, Stephen, Scholl, David, von Huene, Roland, and Wells, Ray, 2013, Alaska earthquake source for the SAFRR tsunami scenario, chapter B, *in* Ross, S.L., and Jones, L.M., eds., The SAFRR (science application for risk reduction) tsunami scenario: U.S. Geological Survey Open-File Report 2013–1170, 40 p. https://pubs.usgs.gov/of/2013/1170/b/

Lander, J.F., 1996, Tsunamis affecting Alaska, 1737–1996: Boulder, CO, National Oceanic and Atmospheric Administration, National Geophysical Data Center (NGDC), Key to Geophysical Research Documentation, v. 31, 155 p.

Larsen, C.F., Motyka, R.J., Freymueller, J.T., Echelmeyer, K.A., and Ivins, E.R., 2004, Rapid uplift of southern Alaska caused by recent ice loss: Geophysical Journal International, v. 158, no. 3, p. 1,118–1,133. https://doi.org/10.1111/j.1365-246X.2004.02356.x

Liu, C., Lay, T., Xiong, X., and Wen, Y., 2020, Rupture of the 2020 M_W 7.8 earthquake in the Shumagin gap inferred from seismic and geodetic observations: Geophysical Research Letters, v. 47, e2020GL090806. https://doi.org/10.1029/2020GL090806

Lopez, A.M., and Okal, E.A., 2006, A seismological reassessment of the source of the 1946 Aleutian 'tsunami' earthquake: Geophysical Journal International, v. 165, no. 3, p. 835–849. https://doi.org/10.1111/j.1365-246X.2006.02899.x

Moss, R.E.S., and Travasarou, Thaleia, 2006, Tsunamigenic probabilistic fault displacement hazard analysis for subduction zones—Proceedings of the 8th U.S. National Conference on Earthquake Engineering: Earthquake Engineering Research Institute, Paper 238, 9 p.

National Geophysical Data Center/World Data Service: NCEI/WDS Global Historical Tsunami Database, NOAA National Centers for Environmental Information. https://doi.org/10.7289/V5PN93H7

National Tsunami Hazard Mapping Program (NTHMP), 2010, Guidelines and best practices for tsunami inundation modeling for evacuation planning: National Oceanic and Atmospheric Administration (NOAA), NTHMP Mapping & Modeling Subcommittee, 4 p.

———2012, Proceedings and results of the 2011 NTHMP Model Benchmarking Workshop: Boulder, CO, U.S. Department of Commerce/NOAA/NTHMP, NOAA Special Report, 436 p.

Nicolsky, D.J., Suleimani, E.N., Combellick, R.A., and Hansen, R.A., 2011a, Tsunami inundation maps of Whittier and western Passage Canal, Alaska: Alaska Division of Geological & Geophysical Surveys Report of Investigation 2011-7, 65 p. https://doi.org/10.14509/23244

Nicolsky, D.J., Suleimani, E.N., Freymueller, J.T., and Koehler, R.D., 2015, Tsunami inundation maps of Fox Islands communities, including Dutch Harbor and Akutan, Alaska: Alaska Division of Geological & Geophysical Surveys Report of Investigation 2015-5, 67 p., 2 sheets, scale 1:12,500. https://doi.org/10.14509/29414

Nicolsky, D.J., Suleimani, E.N., Haeussler, P.J., Ryan, H.F., Koehler, R.D., Combellick, R.A., and Hansen, R.A., 2013, Tsunami inundation maps of Port Valdez, Alaska: Alaska Division of Geological & Geophysical Surveys Report of Investigation 2013-1, 77 p., 1 sheet, scale 1:12,500. https://doi.org/10.14509/25055

Nicolsky, D.J., Suleimani, E.N., and Hansen, R.A., 2011b, Validation and verification of a numerical model for tsunami propagation and runup: Pure and Applied Geophysics, v. 168, no. 6, p. 1,199–1,222. https://doi.org/10.1007/s00024-010-0231-9

Nicolsky, D.J., Suleimani, E.N., and Koehler, R.D., 2014, Tsunami inundation maps of Cordova and Tatitlek, Alaska: Alaska Division of Geological & Geophysical Surveys Report of Investigation 2014-1, 49 p. https://doi.org/10.14509/27241

———2016, Tsunami inundation maps for the communities of Chignik and Chignik Lagoon, Alaska: Alaska Division of Geological & Geophysical Surveys Report of Investigation 2016-8, 48 p., 2 sheets, scale 1:12,500. https://doi.org/10.14509/29675

Nicolsky, D.J., Suleimani, E.N., Koehler, R.D., and Salisbury, J.B., 2017, Tsunami inundation maps for Juneau, Alaska: Alaska Division of Geological & Geophysical Surveys Report of Investigation 2017-9, 66 p., 5 sheets. https://doi.org/10.14509/29741

Okada, Yoshimitsu, 1985, Surface deformation due to shear and tensile faults in a half-space: Bulletin of the Seismological Society of America, v. 75, no. 4, p. 1,135–1,154.

Oppenheimer, Michael, Glavovic, B.C., Hinkel, Jochen, van de Wal, Roderik, Magnan, A.K., Abd-Elgawad, Amro, Cai, Rongshuo, Cifuentes-Jara, Miguel, DeConto, R.M., Ghosh, Tuhin, Hay, John, Isla, Federico, Marzeion, Ben, Meyssignac, Benoit, and Sebesvari, Zita, 2019, Sea level rise implications for low-lying islands, coasts and communities, *in* Pörtner, H.-O., Roberts, D.C., Masson-Delmotte, V., Zhai, P., Tignor, M., Poloczanska, E., Mintenbeck, K., Alegría, A., Nicolai, M., Okem, A., Petzoid, J., Rama, B., Weyer, N.M., eds., IPCC Special Report on the ocean and cryosphere in a changing climate, 126 p. https://www.ipcc.ch/site/assets/uploads/sites/3/2019/11/08_SROCC_Ch04_FINAL.pdf

Page, R.A., Biswas, N.N., Lahr, J.C., and Pulpan, Hans, 1991, Seismicity of continental Alaska, *in* Slemmons, D.B., Engdahl, E.R., Zoback, M.D., and Blackwell, D.D., eds., Neotectonics of North America: Boulder, Colorado, Geological Society of America, Decade Map v. 1, p. 47–68.

Papazachos, B.C., Scordilis, E.M., Panagiotopoulos, D.G., Papazachos, C.B., and Karakaisis, G.F., 2005, Global relations between seismic fault parameters and moment magnitude of earthquakes: Bulletin of the Geological Society of Greece, v. 36, p. 1,482–1,489.

Ryan, Holly, von Huene, Roland, Scholl, Dave, and Kirby, Steve, 2012, Tsunami hazards to U.S. coasts from giant earthquakes in Alaska: Eos American Geophysical Union, v. 93, no. 19, 185 p.

Shirzaei, Manoochehr, Freymueller, Jeffrey, Törnqvist, T.E., Galloway, D.L., Dura, Tina, and Minderhoud, P.S.J., 2021, Measuring, modelling and projecting coastal land subsidence: Nature Reviews Earth & Environment, v. 2, p. 40–58. https://doi.org/10.1038/s43017-020-00115-x

Stein, Seth, and Okal, E.A., 2007, Ultralong period seismic study of the December 2004 Indian Ocean earthquake and implications for regional tectonics and the subduction process: Bulletin of the Seismological Society of America, v. 97, no. 1A, p. S279–S295. https://doi.org/10.1785/0120050617

Suleimani, E.N., Nicolsky, D.J., and Koehler, R.D., 2013, Tsunami inundation maps of Sitka, Alaska: Alaska Division of Geological & Geophysical Surveys Report of Investigation 2013-3, 76 p., 1 sheet, scale 1:250,000. https://doi.org/10.14509/26671

———2015, Tsunami inundation maps of Elfin Cove, Gustavus, and Hoonah, Alaska: Alaska Division of Geological & Geophysical Surveys Report of Investigation 2015-1, 79 p. https://doi.org/10.14509/29404

———2017, Updated tsunami inundation maps of the Kodiak area, Alaska: Alaska Division of Geological & Geophysical Surveys Report of Investigation 2017-8, 38 p., 10 sheets. https://doi.org/10.14509/29740

Suleimani, E.N., Nicolsky, D.J., Koehler, R.D., Freymueller, J.T., and Macpherson, A.E., 2016, Tsunami inundation maps for King Cove and Cold Bay communities, Alaska: Alaska Division of Geological & Geophysical Surveys Report of Investigation 2016-1, 73 p., 2 sheets, scale 1:12,500. https://doi.org/10.14509/29565

Suleimani, E.N., Nicolsky, D.J., West, D.A., Combellick, R.A., and Hansen, R.A., 2010, Tsunami inundation maps of Seward and northern Resurrection Bay, Alaska: Alaska Division of Geological & Geophysical Surveys Report of Investigation 2010-1, 47 p., 3 sheets, scale 1:12,500. https://doi.org/10.14509/21001

Synolakis, C.E., Bernard, E.N., Titov, V.V., Kânoğlu, Utku, and González, F.I., 2007, Standards, criteria, and procedures for NOAA evaluation of tsunami numerical models: National Oceanic and Atmospheric Administration Technical Memorandum OAR PMEL-135, 55 p. https://www.pmel.noaa.gov/pubs/PDF/syno3053/syno3053.pdf

Wang, Kelin, Sun, Tianhaozhe, Brown, Lonn, Hino, Ryota, Tomita, Fumiaki, Kido, Moyoyuki, Iinuma, Takeshi, Kodaira, Shuichi, and Fujiwara, Toshiya, 2018, Learning from crustal deformation associated with the M9 2011 Tohoku-oki earthquake: Geosphere, v. 14, no. 2, p. 552–571. https://doi.org/10.1130/GES01531.1

Wang, Kelin, Wells, R.E., Mazzotti, Stephane, Hyndman, R.D., and Sagiya, Takeshi, 2003, A revised dislocation model of interseismic deformation of the Cascadia subduction zone: Journal of Geophysical Research, v. 108, no. B1, p. 2,026–2,038. https://doi.org/10.1029/2001JB001227

Witter, R.C., Briggs, R.W., Engelhart, S.E., Gelfenbaum, G., Koehler, R.D., and Barnhart, W.D., 2014, Little late Holocene strain accumulation and release on the Aleutian megathrust below the Shumagin Islands, Alaska: Geophysical Research Letters, v. 41, no. 7, p. 2,359–2,367. https://doi.org/10.1002/2014GL059393

Zhao, Bin, Bürgmann, Roland, Wang, Dongzhen, Zhang, Jian, Yu, Jiansheng, and Li, Qi, 2022, Aseismic slip and recent ruptures of persistent asperities along the Alaska-Aleutian subduction zone: Nature Communications, v. 13, no. 3,098, 12 p. https://doi.org/10.1038/s41467-022-30883-7

APPENDIX A

Table A1. Location of time series points in and around False Pass. The maximum water depth above ground is provided for onshore locations (S), whereas the maximum water level above the pre-earthquake MHHW is provided for offshore (O) locations.

#	Label	S / O	Longitude (°W)	Latitude (°N)	Min. elevation/ depth (m)
1	Ikatan Bay	O	-163.356389	54.798889	37.9
2	Isanotski Strait	O	-163.394444	54.849167	28.5
3	Ferry Dock	O	-163.406667	54.854444	5.3
4	Unimak Drive	O	-163.404444	54.845000	-0.1
5	Battery Road	S	-163.408889	54.853889	-0.7
6	Boardwalk	S	-163.408889	54.855000	-0.7
7	Four Winds	S	-163.415556	54.860278	-0.6
8	Tribal Warehouse	S	-163.413333	54.862500	-0.5
9	Harbor	O	-163.408611	54.866111	6.8
10	Grocery Store	S	-163.410000	54.866667	0.5
11	Silver Bay Seafoods	S	-163.407222	54.868889	-0.4
12	City Dock	O	-163.410556	54.861944	10.5
13	Breakwaters	O	-163.406944	54.866944	1.2
14	Nichols Point	S	-163.381389	54.850556	-0.8

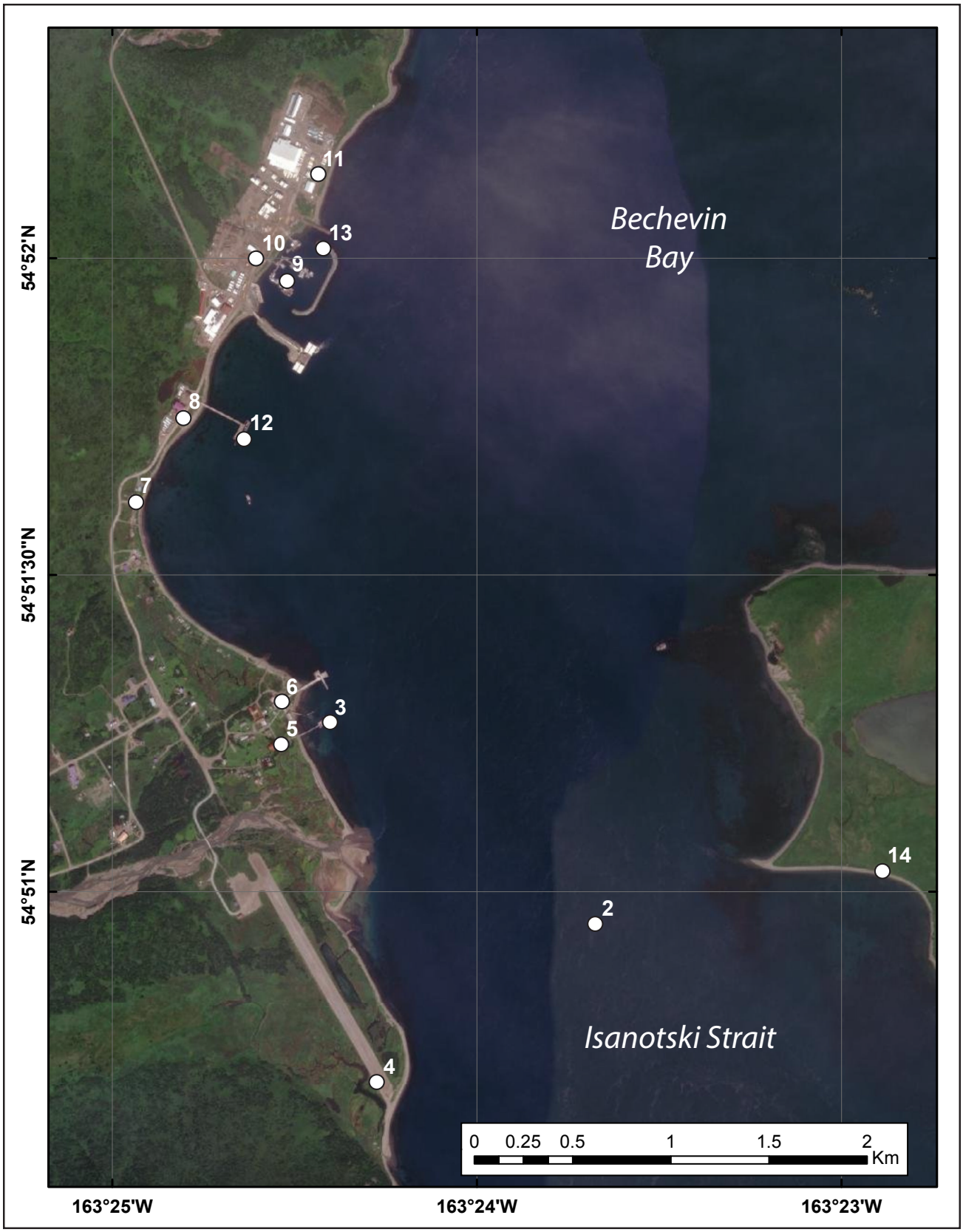

Figure A1. Locations of time series points in and around False Pass. The longitude and latitude locations of the time series points are listed in table A1.

Table A2. Maximum water depth for all tsunami scenarios at time series points in and around False Pass.

#	Label	Maximum water depth above ground/sea level (meters)																	
		Scenario																	
		1	2	3	4	5	6	7	8	9	10	11	12	13	14	15	16	17	18
1	Ikatan Bay	8.1	10.7	9.2	8.2	2	5.3	1.0	5.6	5.8	6.0	12.2	7.8	5.4	9.9	8.1	9.5	8.8	2.5
2	Isanotski Strait	4.3	6.4	5.0	3.8	1.1	3.2	0.8	3.9	4.0	3.9	7.2	6.7	3.8	4.9	5.5	5.8	6.1	0.9
3	Ferry Dock	4.3	6.0	4.8	3.8	1	2.8	0.7	3.6	3.7	3.7	7.1	5.7	3.9	4.2	5.3	5.3	5.7	0.8
4	Unimak Drive	5.1	6.7	5.7	3.9	1.2	3.4	0.8	4.3	4.4	4.5	7.8	7.0	4.5	5.4	6.7	6.5	6.5	1.0
5	Battery Road	3.4	4.8	4.1	2.5	0	1.7	0	2.6	2.7	2.7	6.3	4.8	3.0	3.3	4.6	4.7	4.9	0
6	Boardwalk	3.4	4.7	4.4	2.6	0	1.4	0	2.2	2.4	2.6	7.0	5.1	2.5	3.0	5.2	5.5	4.7	0
7	Four Winds	3.5	5.1	5.3	2.6	0	2.4	0	3.3	3.7	2.6	10.1	6.1	3.9	4.2	8.1	7.6	7.0	0
8	Tribal Warehouse	3.4	4.1	4.2	2.5	0	2.3	0	3.2	3.3	2.7	7.2	5.3	3.7	3.4	5.8	5.7	5.6	0
9	Harbor	3.6	4.8	4.6	3.9	0.9	2.8	0.7	3.5	3.5	3.1	6.1	5.1	3.8	3.9	4.9	4.9	5.4	0.7
10	Grocery Store	1.5	2.5	2.2	1.4	0	0.4	0	1.3	1.3	0.9	4.4	2.8	1.5	1.7	3.1	3.1	3.3	0
11	Silver Bay Seafoods	1.3	3.0	2.7	1.5	0	0.5	0	1.2	1.2	0.8	3.7	2.7	1.5	1.7	3.0	2.9	3.2	0
12	City Dock	4.3	5.4	4.8	3.9	0.9	3.0	0.7	3.9	4.0	3.5	7.7	5.8	4.3	4.6	5.9	5.9	6.3	0.7
13	Breakwaters	3.7	4.7	4.5	3.9	0.9	3.0	0.7	3.5	3.6	3.2	6.4	5.0	3.8	3.9	5.5	5.5	5.3	0.7
14	Nichols Point	4.0	6.5	4.5	3.1	0	2.6	0	3.7	3.9	3.9	7.7	6.4	4.2	4.6	5.5	6.0	6.1	0

Table A3. Maximum water velocities for all tsunami scenarios at time series points in and around False Pass.

#	Label	Maximum water depth above ground/sea level (meters)																	
		Scenario																	
		1	2	3	4	5	6	7	8	9	10	11	12	13	14	15	16	17	18
1	Ikatan Bay	2.4	2.8	2.2	4.0	0.6	2.0	0.3	1.4	2.1	2.0	3.0	3.1	1.6	2.9	2.3	2.4	3.8	0.6
2	Isanotski Strait	6.2	6.2	6.2	6.8	1.7	5.6	1.0	4.9	6.4	6.3	7.7	6.9	4.1	6.6	5.4	6.2	7.4	2.7
3	Ferry Dock	5.1	5.4	5.5	5.9	1.5	5.3	1.0	3.9	6.1	5.1	5.3	6.5	3.4	6.3	4.1	5.4	5.6	2.2
4	Unimak Drive	4.7	5.0	5.0	3.8	1.5	3.1	1.1	3.6	3.5	3.7	6.5	4.6	3.8	4.2	5.6	5.2	4.5	1.3
5	Battery Road	3.8	4.1	2.8	2.0	0	3.2	0	3.2	3.1	3.1	11.1	4.8	3.2	4.9	5.1	3.9	3.5	0
6	Boardwalk	3.9	4.3	4.3	2.9	0	3.0	0	3.2	3.2	3.2	10	4.7	3.5	4.3	8.3	7	4.5	0
7	Four Winds	3.6	7.9	6.6	1.5	0	3.5	0	4.4	4.9	3.4	14.9	6.2	5.2	2.7	11.9	10.9	4.2	0
8	Tribal Warehouse	3.7	5.1	4.3	2.9	0	3.1	0	3.5	3.6	3	8.9	4.7	3.7	4.6	7.8	6.7	6.5	0
9	Harbor	1.1	1.5	1.6	0.5	0.1	0.8	0.2	0.9	1.1	0.7	2.8	1.8	1.2	1	2.7	2.2	1.7	0.1
10	Grocery Store	2.6	3.9	3.3	2.0	0	1.4	0	2.6	3.0	1.8	5.2	4.0	3.1	3.1	4.1	5.3	4.2	0
11	Silver Bay Seafoods	1.9	3.2	3.5	1.2	0	1.5	0	1.8	1.9	2.0	9.0	3.5	2.0	2.2	5.2	5.2	3.0	0
12	City Dock	1.8	2.2	1.8	1.5	0.6	1.6	0.4	1.5	1.8	1.7	3.5	2.3	1.7	1.8	2.8	2.6	2.7	0.8
13	Breakwaters	1.3	1.6	1.6	1.4	0	0.9	0	1.3	1.3	1.1	2.7	2.0	1.4	1.3	2.2	2.3	2.0	0
14	Nichols Point	7.9	10.5	5.9	3.5	0	3.6	0	5.5	10	5.9	8.8	8.4	4.8	5.2	7.1	7.4	8.5	0

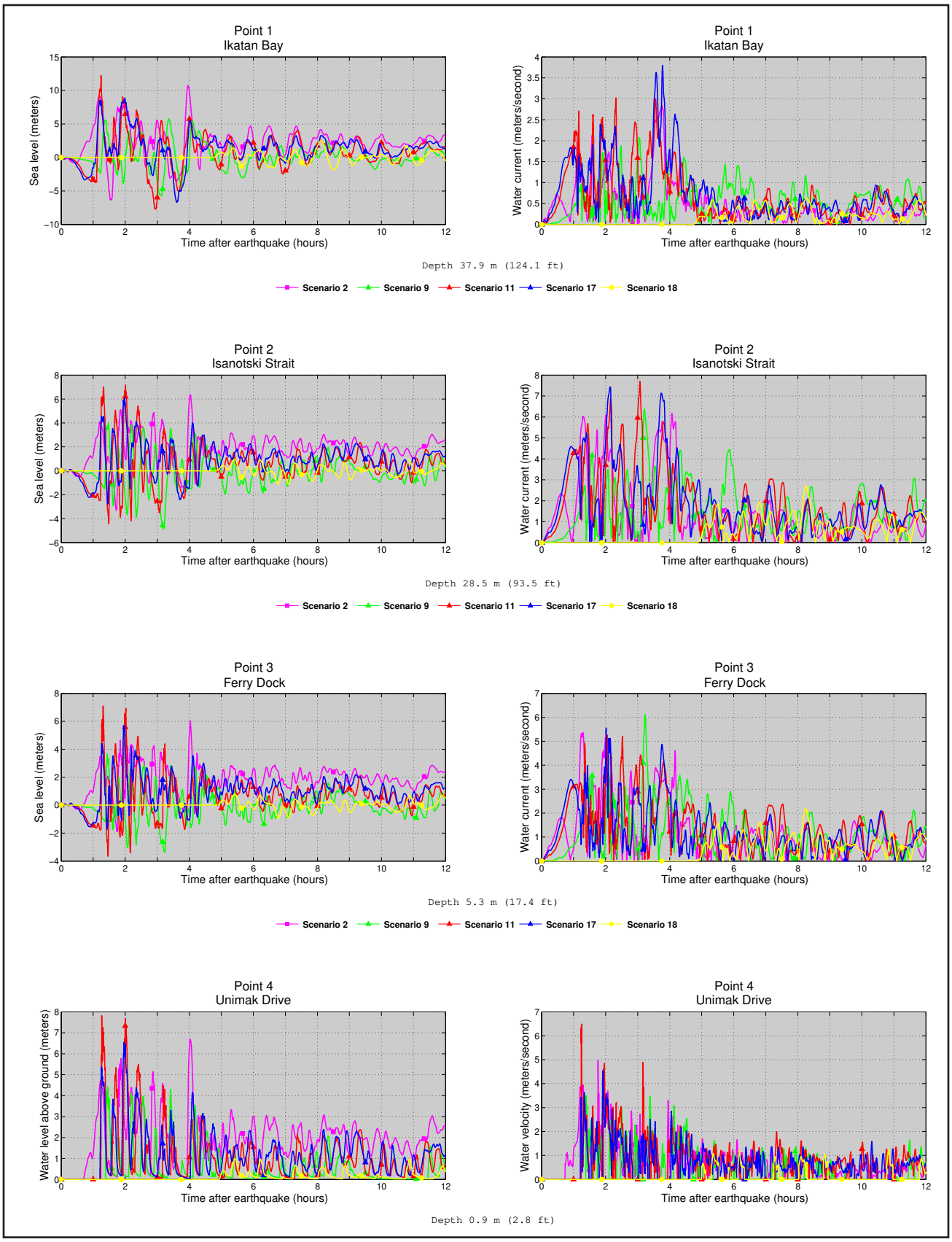

Figure A2. Time series of water level (left column) and velocity (right column) for selected scenarios at locations shown in figure A1. Elevations of onshore locations and ocean depth at offshore locations are given based on the pre-earthquake MHHW datum.

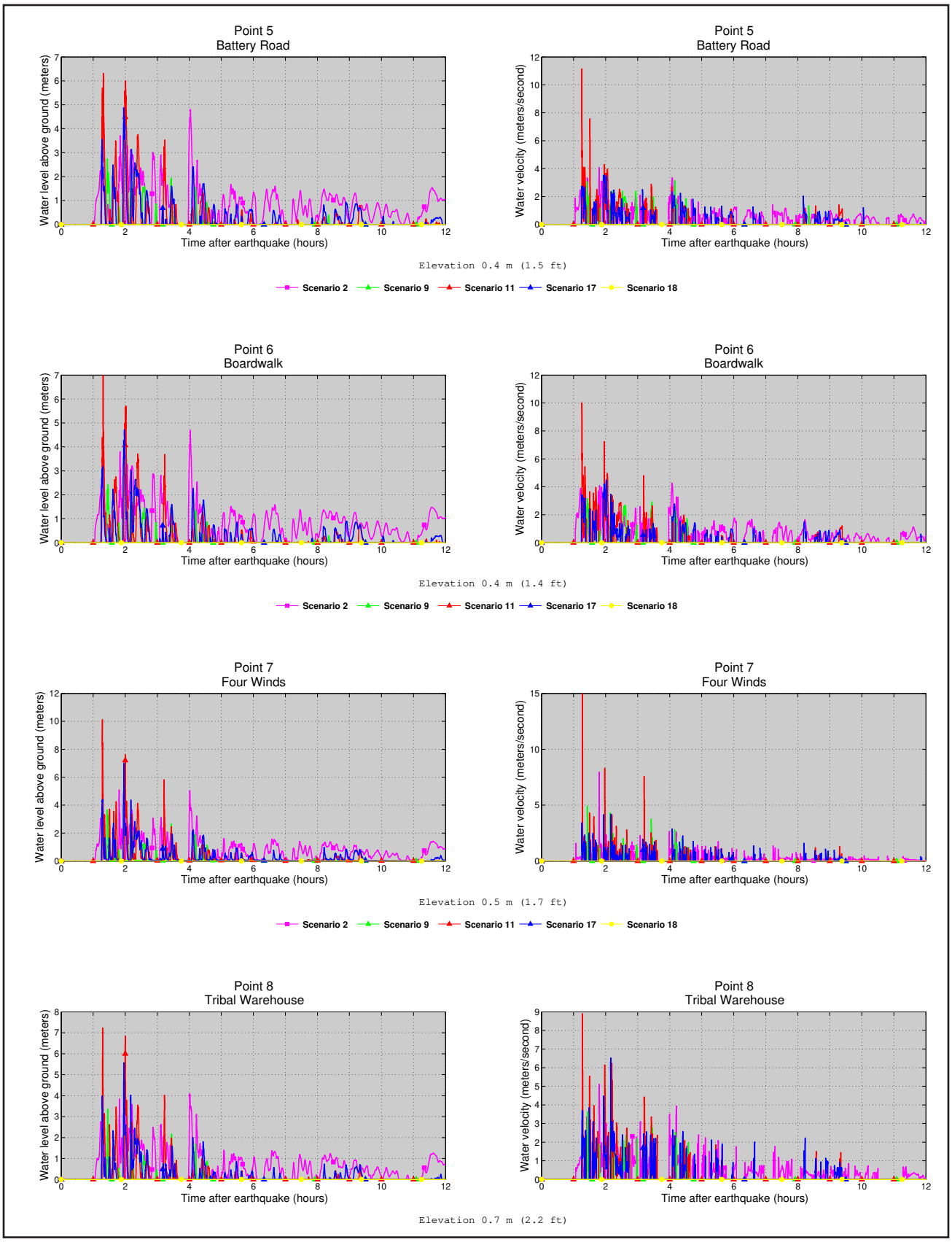

Figure A2, continued. Time series of water level (left column) and velocity (right column) for selected scenarios at locations shown in figure A1. Elevations of onshore locations and ocean depth at offshore locations are given based on the pre-earthquake MHHW datum.

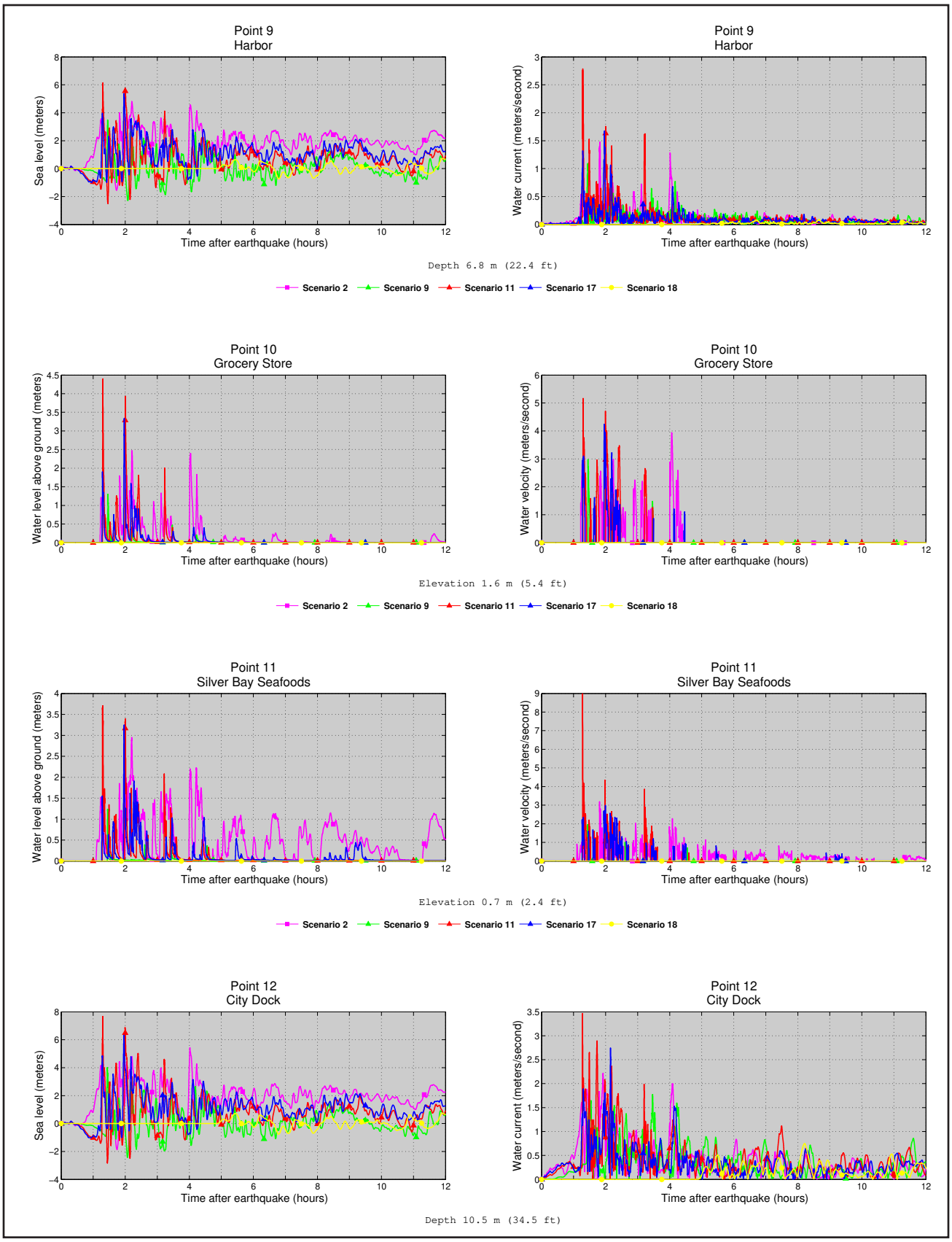

Figure A2, continued. Time series of water level (left column) and velocity (right column) for selected scenarios at locations shown in figure A1. Elevations of onshore locations and ocean depth at offshore locations are given based on the pre-earthquake MHHW datum.

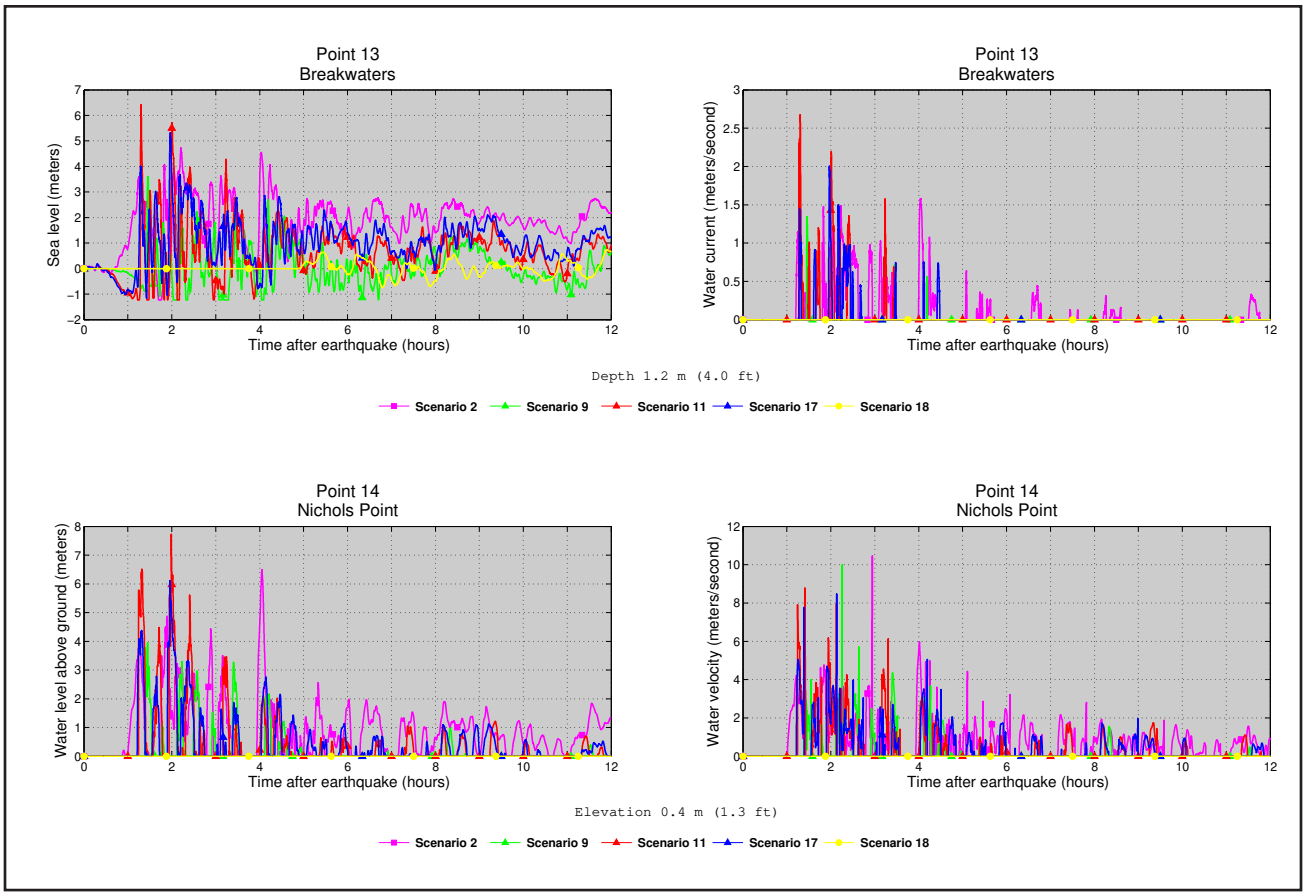

Figure A2, continued. Time series of water level (left column) and velocity (right column) for selected scenarios at locations shown in figure A1. Elevations of onshore locations and ocean depth at offshore locations are given based on the pre-earthquake MHHW datum.